Decentralized Event-Based Controllers for Robust Stabilization of Hybrid Periodic Orbits: Application to Underactuated 3D Bipedal Walking

Kaveh Akbari Hamed and Robert D. Gregg

***Abstract*—Models of bipedal walking are hybrid, with continuous-time dynamics representing the swing phases and discrete-time dynamics representing the impact events. The feedback controllers for these systems can be two-level, including both continuous- and discrete-time (event-based) actions. This paper presents a systematic framework to design decentralized event-based controllers for robust stabilization of hybrid periodic orbits against possible disturbances in discrete-time phases. The properties of the Poincaré return map are investigated to study the orbital input-to-state stability for the closed-loop system with respect to disturbance inputs. An optimization problem involving bilinear matrix inequalities is then presented to design $\mathcal{H}_2$- and $\mathcal{H}_\infty$-optimal decentralized event-based controllers. The power of the proposed framework is finally demonstrated through designing a set of decentralized two-level controllers for underactuated walking of a 3D autonomous bipedal robot with nine degrees of freedom and a decentralization scheme motivated by amputee locomotion with a transpelvic prosthetic leg.**

***Index Terms*—Decentralized Two-Level Controllers, Hybrid Periodic Orbits, Underactuated 3D Bipedal Robots, $\mathcal{H}_2$- and $\mathcal{H}_\infty$-Optimal Event-Based Controllers, Virtual Constraints.**

NOMENCLATURE

x, u, d	Global state variables, global control inputs, discrete-time uncertainty
x_i, u_i	Local state variables and control inputs for the subsystem Σ_i
$\mathcal{O}, \varphi^\star, u^\star$	Periodic orbit, nominal state trajectory and control input on the orbit (see Assumption 1)
θ, Θ	Phasing variable and sequence of its consecutive time-derivatives (see Assumption 2)
$\psi_i^{\text{ct}}, \Psi_i^{\text{ct}}$	Global continuous-time variables and set of global continuous-time variables for the subsystem Σ_i (see Assumption 6)
$\psi_i^{\text{dt}}, \Psi_i^{\text{dt}}$	Global discrete-time variables and set of global discrete-time variables for the subsystem Σ_i (see Assumption 6)
$\Gamma_i, \text{fcn}_i, \Gamma$	Decentralized continuous-time controller and its subfunction for the subsystem Σ_i (see (23)), continuous-time controller (see (6))
$\beta_i, \beta_i^\star, \beta, \beta^\star$	Local event-based parameters and local nominal event-based parameters for the subsystem Σ_i, global event-based parameters and global nominal event-based parameters
$f^{\text{cl}}, f_0^{\text{cl}}, \varphi$	Piecewise-defined closed-loop vector field, its subfunction, and state solution (see (7))
$y_i, H_i, \hat{H}_i$	Local output function and output matrices for the subsystem Σ_i (see (24))
e, π, ζ	State variables for the event-based controller, event-based control law, event-based dynamics (see (8) and (9))
e_i, π_i, ζ_i	State variables for the decentralized event-based controller, decentralized event-based control law, decentralized event-based dynamics (see (27) and (28))
$K_i, \hat{K}_i, \tilde{K}_i$	Local gains for the subsystem Σ_i (see (29))
$\mathcal{F}^-, \mathcal{F}^+, P$	Pre-update flow map (see (12)), post-update flow map (see (13)), Poincaré map (see (14))
χ, Q, Z, μ	Decision variables for the BMI optimization problems (see Proposition 2)
$\eta_i, \hat{\eta}_i, \tilde{\eta}_i$	Decision variables for the BMI optimization problems (see Proposition 2)

This material is based upon work supported by the National Science Foundation under Grant Number 1637704. The content is solely the responsibility of the authors and does not necessarily represent the official views of the NSF. Robert D. Gregg, IV, Ph.D., holds a Career Award at the Scientific Interface from the Burroughs Wellcome Fund.

K. Akbari Hamed (Corresponding Author) is with the Department of Mechanical Engineering, Virginia Tech, Blacksburg, VA 24061 USA (Email: kavehakbarihamed@vt.edu). R. D. Gregg is with the Departments of Bioengineering and Mechanical Engineering, University of Texas at Dallas, Richardson, TX 75080-3021 USA (Email: rgregg@ieee.org).

I. INTRODUCTION

THE OBJECTIVE of this paper is to present a systematic framework to design decentralized *event-based* controllers for robust stabilization of periodic orbits for hybrid systems in the presence of uncertainties in discrete-time dynamics. A class of decentralized, nonlinear, and two-level controllers is proposed. The properties of the Poincaré return map are studied to (1) study the orbital input-to-state stability (ISS) of periodic orbits and (2) present an optimization problem based on bilinear matrix inequalities (BMIs) to solve for $\mathcal{H}_2$- and $\mathcal{H}_\infty$-optimal decentralized event-based controllers. The theoretical innovations are applied to design decentralized two-level controllers for walking gaits of an underactuated 3D bipedal robot with 9 degrees of freedom (DOFs) and 6 actuators. It is shown that the proposed two-level control solutions can reduce the $\mathcal{H}_2$ and $\mathcal{H}_\infty$ norms of the linearized Poincaré map by 45% compared to one-level controllers.

Previous work in legged robot locomotion used *centralized* multi-level feedback control architectures to stabilize periodic orbits [1]–[22], but in many cases decentralization could be advantageous or even necessary. In particular, centralized nonlinear control methods do not easily scale with the dozens

of DOFs designed into modern legged robots. Popular control methods for dynamic walking based on feedback linearization [23] require the inversion of a state-dependent "decoupling" matrix in real time, but the computational complexity of this operation scales quadratically with matrix dimension, i.e., the number of robot DOFs. Moreover, inverting the full decoupling matrix distributes (and amplifies) local modeling errors and sensor noise across all DOFs in the closed-loop dynamics. These problems would be avoided by decentralizing the computation and control into an interconnected network of subsystems, each using their own model-based control law with locally available sensor feedback. Moreover, decentralized control methods are necessary for application to wearable robots like prosthetic legs and exoskeletons, which do not have access to models or feedback for the entire human body.

The most basic tool to investigate the stability of hybrid periodic orbits is the Poincaré return map [2], [20], [24], [25], which describes the evolution of the hybrid system on a hyper-surface transversal to the orbit, referred to as the Poincaré section. The Poincaré return map has been commonly used to design two-level controllers for models of legged robots [8], [12], [13], [19]–[21], [26]–[31]. In this approach, continuous-time controllers are parameterized by a set of adjustable parameters. The parameters are then updated in a stride-to-stride manner by event-based controllers when state solutions cross the Poincaré section. Event-based controllers are mainly designed in a centralized manner using linear matrix inequalities (LMIs) [20] or discrete linear-quadratic regulators [23, Chapter 7], [26]. However, these approaches *cannot* be transferred to the design of decentralized event-based controllers for interconnected hybrid subsystems.

To the best of our knowledge, there is currently *no* systematic algorithm to design decentralized event-based controllers for the hybrid models of legged robots. State-of-the-art decentralized controllers for large-scale systems pertain to the stabilization of *equilibrium points* for ordinary differential equations (ODEs) and *not* periodic orbits of hybrid dynamical systems [24], [32]–[35]. Most of the existing control strategies for powered prosthetic legs employ hand-tuned *linear* decentralized feedback control laws that change based on discrete phases of gait to track reference joint kinematics [36], impedances [37], and/or joint torques [38]. These finite state machines are susceptible to perturbations that cause the wrong controller to be employed at the wrong time, underlining the need for robust, nonlinear decentralized multi-level controllers for prostheses and exoskeletons. Decentralized partial feedback linearization schemes were developed for powered prosthetic legs in [39]–[41] and subsequently for lower-limb exoskeletons in [42], but these methods either rely on measurements of human interaction forces or assume the human subsystem remains on a predefined orbit. Our previous work in [43], [44] avoids these drawbacks by solving optimization problems to systematically design decentralized *continuous-time* controllers (i.e., one-level controllers) that only share a common phasing variable between subsystems (e.g., [45]). However, this approach did *not* include decentralized event-based updates to the parameters of the continuous-time controllers in response to discrete-time disturbances, e.g., inaccuracies in the contact model. The integration of decentralized event-based *and* continuous-time controllers would increase the robustness of underactuated walking gaits against the impact model uncertainties.

The contributions of this paper are as follows: (1) A class of decentralized two-level controllers is first presented, in which the parameters of decentralized continuous-time controllers are updated by *static* or *dynamic* decentralized event-based controllers. (2) The properties of the Poincaré return map are then studied to investigate the orbital ISS property for hybrid periodic orbits with respect to disturbance inputs in the discrete-time dynamics. (3) A BMI optimization framework is presented to solve for $\mathcal{H}_2$- and $\mathcal{H}_\infty$-optimal decentralized event-based controllers. (4) A systematic numerical approach is presented to compute the Jacobian linearization of the Poincaré return map. (5) The proposed decentralized two-level controllers are also numerically validated on an autonomous 3D bipedal robot with 9 DOFs and 6 actuators. (6) It is shown that using the proposed decentralized two-level control solutions, the $\mathcal{H}_2$ and $\mathcal{H}_\infty$ norms can be reduced by 45% compared to the one-level decentralized controllers in our previous work [43]. Finally, the closed-loop model is shown to be robust against parametric and nonparametric uncertainties arising from contact models.

Our previous work in [43], [44] only applied $\mathcal{H}_2$-optimal decentralized *continuous-time* controllers for models of bipedal walking, but it did *not* consider the design of decentralized event-based (i.e., discrete-time) controllers. In order to increase the robustness of the closed-loop system, the current paper addresses the design of two-level controllers. In particular, the current paper adds *higher-level event-based controllers* that update the parameters of lower-level continuous-time controllers in a step-by-step manner. The design of decentralized event-based controllers is a hard problem and cannot be addressed using the LMI formulations of [20], [46] or the BMI formulations of [43], [44]. We first establish a connection between the ISS property of limit cycles and their exponential stability behavior to study the effect of disturbances on the orbital distance from state solutions to hybrid periodic orbits. We then present a novel BMI formulation to address the design of $\mathcal{H}_2$- and $\mathcal{H}_\infty$-optimal decentralized event-based controllers. Our results show that this two-level control strategy significantly improves the robustness of the closed-loop system against impact model uncertainties compared to the one-level control strategy in [43], [44].

This paper is organized as follows. Section II presents hybrid models of walking. Section III develops two-level controllers and addresses the orbital ISS property. Section IV develops decentralized two-level controllers. The robust stabilization problem and $\mathcal{H}_2$- and $\mathcal{H}_\infty$-optimal decentralized event-based controllers are addressed in Section V. Section VI presents a numerical approach for the Jacobian linearization of the Poincaré map. Section VII applies the theoretical results to the hybrid models of bipedal walking and presents numerical simulations. Section VIII presents concluding remarks.

Notation: We shall let $\mathbb{R}$, $\mathbb{R}_{>0}$, and $\mathbb{R}_{\geq 0}$ denote the sets of real, positive, and nonnegative real numbers, respectively. $\mathbb{R}^n$ represents the n-dimensional Euclidean space. For any vector

$x \in \mathbb{R}^n$, we use the notation $\|x\|$ to represent the norm of x. For any $A \in \mathbb{R}^{n\times n}$, we use the notation $A > 0$ to denote that A is a positive definite matrix. In addition, the trace and transpose of a matrix A are shown by trace(A) and $A^\top$, respectively. The Frobenius norm and vectorization operator of a given matrix $A \in \mathbb{R}^{m\times n}$ are represented by $\|A\|_{\mathrm{F}}$ and vec (A). The set closure of a set $\mathcal{O}$ is shown by $\overline{\mathcal{O}}$. For a given $x \in \mathbb{R}^n$ and $\delta > 0$, $\mathcal{N}_\delta(x)$ denotes an open ball centered at x with the radius δ. Moreover, the distance from a point x to a set $\mathcal{O}$ is represented by $\mathrm{dist}(x, \mathcal{O}) := \inf_{a\in\mathcal{O}} \|x - a\|$. For a given manifold $\mathcal{M}$, T$\mathcal{M}$ denotes the tangent bundle of $\mathcal{M}$. The set of continuously differentiable and smooth functions are represented by $\mathcal{C}^1$ and $\mathcal{C}^\infty$, respectively. For a given function $x : \mathbb{R} \to \mathbb{R}^n$, we let $x^-(t)$ and $x^+(t)$ denote the left and right limits of $x(t)$. Finally, the l_p norm of a discrete-time signal $\{x[k]\}_{k=0}^\infty$ is represented by $\|x\|_{l_p}$. A continuous function $\alpha : [0, a) \to \mathbb{R}_{\geq 0}$ is said to be a $\mathcal{K}$ function if it is strictly increasing and $\alpha(0) = 0$. It is said to be a $\mathcal{K}_\infty$ function if $a = \infty$ and $\lim_{x\to\infty} \alpha(x) = \infty$. A continuous function $\rho : [0, a) \times [0, \infty) \to \mathbb{R}_{\geq 0}$ is said to be a $\mathcal{KL}$ function if, for each fixed y, $\rho(x, y)$ is a $\mathcal{K}$ function with respect to x and, for each fixed x, $\rho(x, y)$ is decreasing with respect to y and $\lim_{y\to\infty} \rho(x, y) = 0$ [47].

II. Hybrid Model

We consider single-phase hybrid dynamical systems arising from bipedal walking as follows

$$\Sigma : \begin{cases} \dot{x} = f(x) + g(x)\, u, & x^- \notin \mathcal{S} \\ x^+ = \Delta(x^-) + d, & x^- \in \mathcal{S}, \end{cases} \tag{1}$$

in which $x \in \mathcal{X} \subset \mathbb{R}^n$ and $u \in \mathcal{U} \subset \mathbb{R}^m$ denote the *global state variables* and *global control inputs*, respectively. The *global state manifold* and *admissible set of global control inputs* are represented by $\mathcal{X} \subset \mathbb{R}^n$ and $\mathcal{U} \subset \mathbb{R}^m$ for some positive integers $n > m$. The evolution of the system during the continuous-time phase is described by the state equation $\dot{x} = f(x) + g(x)\, u$, where $f : \mathcal{X} \to \mathrm{T}\mathcal{X}$ is a smooth (i.e., $\mathcal{C}^\infty$) vector field. The columns of the g matrix are denoted by $g_j : \mathcal{X} \to \mathrm{T}\mathcal{X}$ for $1 \leq j \leq m$ and assumed to be $\mathcal{C}^\infty$. The evolution of the system during the discrete-time phase is then described by the *instantaneous mapping* $x^+ = \Delta(x^-) + d$, where $\Delta : \mathcal{X} \to \mathcal{X}$ denotes a $\mathcal{C}^\infty$ *reset map*. In this paper, we assume that there is a *bounded*, *additive*, and *unknown* uncertainty in the reset map, shown by $d \in \mathcal{D}$. The *set of admissible disturbance inputs* is represented by $\mathcal{D} \subset \mathbb{R}^n$ that is assumed to be a bounded, connected, and open neighborhood of the origin $d = 0$. Finally, the guard of the hybrid system, referred to as the *switching manifold*, is given by the $(n-1)$-dimensional manifold $\mathcal{S} := \{x \in \mathcal{X} \,|\, s(x) = 0, \varsigma(x) < 0\}$ on which the state solutions of the hybrid system (1) undergo an abrupt change according to the reset law $x^+ = \Delta(x^-) + d$. In our notation, $s : \mathcal{X} \to \mathbb{R}$ is a $\mathcal{C}^\infty$ function, referred to as the *switching function*, that satisfies the condition[1] $\frac{\partial s}{\partial x}(x) \neq 0$ for all $x \in \mathcal{S}$. Furthermore, $\varsigma : \mathcal{X} \to \mathbb{R}$ is a $\mathcal{C}^\infty$ function to specify feasible switchings by $\varsigma(x) < 0$. According to [2], the state solution of (1) is defined as follows.

Definition 1 (State Solution): The function $\varphi : [0, t_f) \to \mathcal{X}$, $t_f \in \mathbb{R}_{>0} \cup \{\infty\}$ is said to be a *solution* to (1) if

1) $\varphi(t)$ is right continuous on $[0, t_f)$;
2) The left and right limits $\varphi^-(t) := \lim_{\tau\nearrow t} \varphi(\tau)$ and $\varphi^+(t) := \lim_{\tau\searrow t} \varphi(\tau)$ exist for every $t \in (0, t_f)$; and
3) There exist (i) a closed discrete subset $\mathcal{T} := \{t_0 < t_1 < t_2 < \cdots\} \subset [0, t_f)$, referred to as the switching times, (ii) a right continuous control input $u : [0, t_f) \to \mathcal{U}$, and (iii) a discrete-time disturbance input $d : \mathcal{T} \to \mathcal{D}$ such that, (a) for every $t \in [0, t_f) \setminus \mathcal{T}$, $\varphi(t)$ is differentiable, $\dot{\varphi}(t) = f(\varphi(t)) + g(\varphi(t))\, u(t)$, $\varphi^-(t) \notin \mathcal{S}$, and (b) for $t = t_k \in \mathcal{T}$, $\varphi^-(t) \in \mathcal{S}$ and $\varphi^+(t) = \Delta(\varphi^-(t)) + d_k$, where $d_k := d(t_k)$.

Throughout this paper, we shall assume that there exists a period-one orbit for the hybrid model (1) in the absence of the external input d that is transversal to the switching manifold $\mathcal{S}$. In particular, we make the following assumption.

Assumption 1: (Transversal Period-One Orbit): There exist (i) a finite period $T^\star > 0$ (referred to as the *fundamental period*), (ii) a *nominal global control input* $u^\star : [0, \infty) \to \mathcal{U}$, (iii) a *nominal global state solution* $\varphi^\star : [0, \infty) \to \mathcal{X}$, and (iv) a nonempty set of switching times $\mathcal{T}$ such that (1) $\varphi^\star(t + T^\star) = \varphi^\star(t)$ for all $t \geq 0$ in the absence of the external disturbance input d, and (2) $\varphi^\star(t)$ and $u^\star(t)$ are smooth for every $t \notin \mathcal{T}$. Then $\mathcal{O} := \{x = \varphi^\star(t) \,|\, 0 \leq t < T^\star\}$ is a *period-one orbit* of (1). In addition, we assume that $\mathcal{O}$ is *transversal* to the switching manifold $\mathcal{S}$, i.e.,

$$\{x^\star\} := \{\varphi^{\star-}(T^\star)\} := \overline{\mathcal{O}} \cap \mathcal{S} \tag{2}$$

is a singleton and $\frac{\partial s}{\partial x}(x^\star)\left(f(x^\star) + g(x^\star)\, u^{\star-}(T^\star)\right) \neq 0$, where $\varphi^{\star-}(T^\star)$ and $u^{\star-}(T^\star)$ denote the left limits at $t = T^\star$.

We shall consider the periodic orbit $\mathcal{O}$ as the *desired orbit* to be exponentially/robustly stabilized for the hybrid system (1). In order to develop *time-invariant* and decentralized two-level controllers to stabilize the orbit $\mathcal{O}$, we make use of the concept of a phasing variable.

Assumption 2: (Phasing Variable): There exists a smooth and real-valued function $\theta : \mathcal{X} \to \mathbb{R}$, referred to as the *phasing variable*, that is a strictly increasing function of time on $\overline{\mathcal{O}}$, i.e., $\dot{\theta}(x) > 0$ for all $x \in \overline{\mathcal{O}}$. In addition, it is supposed that the phasing variable has the relative degree $r \geq 1$ with respect to the control input u, that is, the control input u does *not* explicitly appear in the equations of the following vector

$$\Theta(x) := \left(\theta(x), \frac{\mathrm{d}}{\mathrm{d}t}\theta(x), \cdots, \frac{\mathrm{d}^{r-1}}{\mathrm{d}t^{r-1}}\theta(x)\right)^\top \in \mathbb{R}^r. \tag{3}$$

The phasing variable represents the progress of the system (i.e., robot) on the periodic orbit (i.e., walking gait). Reference [48] shows that the existence of a phasing variable follows directly from Assumption 1 on the periodic orbit. Let us denote the evolution of the phasing variable on $\overline{\mathcal{O}}$ by $\theta = \theta^\star(t)$ for $0 \leq t \leq T^\star$. Then, one can express the *desired evolution of the state variables* on the orbit $\mathcal{O}$ in terms of the phasing variable as follows

$$x_{\mathrm{des}}(\theta) := \varphi^\star(t)\Big|_{t=(\theta^\star)^{-1}(\theta)}, \tag{4}$$

[1] The regularity condition $\frac{\partial s}{\partial x}(x) \neq 0$ for all $x \in \mathcal{S}$ guarantees that $\mathcal{S}$ is an $(n-1)$-dimensional embedded submanifold of $\mathcal{X}$.

where the subscript "des" stands for the desired evolution and $t = (\theta^\star)^{-1}(\theta)$ represents the inverse of the strictly monotonic function $\theta = \theta^\star(t)$. In an analogous manner, one can define the *feedforward control input* corresponding to the orbit $\mathcal{O}$ in terms of the phasing variable as $u_{\text{des}}(\theta) := u^\star(t)|_{t=(\theta^\star)^{-1}(\theta)}$. Finally, the minimum and maximum values of θ on the orbit $\overline{\mathcal{O}}$ are expressed by $\theta_{\min} := \min_{x\in\overline{\mathcal{O}}}\theta(x)$ and $\theta_{\max} := \max_{x\in\overline{\mathcal{O}}}\theta(x)$, respectively.

Remark 1: Although most of the existing feedback linearizing controllers for bipedal robots make use of relative degree two holonomic phasing variables and output functions to be regulated (see Section VII-D), there are a few recent results that make use of relative degree one nonholonomic quantities [45], [49], [50]. This motivates the reason for having a general relative degree r in Assumptions 2 and 6.

III. Closed-Loop Hybrid System

This section presents a family of two-level controllers for the model of walking and addresses the Poincaré map and ISS property for the closed-loop system. For the sake of simplicity, the results of this section are presented for controllers that are functions of global state variables. Section IV will decompose the controllers into decentralized controllers.

A. Continuous-Time Controllers

This section presents the continuous-time portion of the two-level controllers. The event-based portion will be presented in Section III-B. We develop a class of *parameterized*, *piecewise-defined*, *continuously differentiable*, and *nonlinear* continuous-time controllers. These controllers are parameterized by a set of *adjustable* parameters, referred to as the *global event-based parameters*. During the continuous-time phase, the parameters are kept constant. However, they are allowed to be updated by *event-based update laws* when state solutions intersect an *event-based manifold*. The event-based manifold can be chosen anywhere within the continuous-time phase (i.e., robotic walking gait). However motivated by [20], [51], we assume that it is taken in the middle of the continuous-time phase (i.e., gait). We denote the *global event-based parameters* by $\beta \in \mathcal{B}$, where $\mathcal{B} \in \mathbb{R}^p$ represents the *admissible set of global event-based parameters* for some positive integer p. The *event-based manifold* is then defined as a level-set of the phasing variable, i.e.,

$$\mathcal{S}^0_{\text{eb}} := \{x \in \mathcal{X} \,|\, \theta(x) = \theta_{\text{eb}}\}, \tag{5}$$

where the subscript "eb" stands for the event-based manifold and the threshold value θ_{eb} is taken as $\theta_{\text{eb}} := \frac{1}{2}(\theta_{\min} + \theta_{\max})$. For later purposes, one can define the sets $\mathcal{S}^-_{\text{eb}} := \{x \in \mathcal{X} \,|\, \theta(x) < \theta_{\text{eb}}\}$ and $\mathcal{S}^+_{\text{eb}} := \{x \in \mathcal{X} \,|\, \theta(x) > \theta_{\text{eb}}\}$ to split the state space as $\mathcal{X} = \mathcal{S}^-_{\text{eb}} \cup \mathcal{S}^0_{\text{eb}} \cup \mathcal{S}^+_{\text{eb}}$.

Now we are in a position to present the class of parameterized continuous-time controllers $\Gamma : \mathcal{X} \times \mathcal{B} \to \mathcal{U}$ by the following piecewise-defined policy

$$\Gamma(x,\beta) := \begin{cases} \text{fcn}(x,\beta^\star), & x \in \mathcal{S}^-_{\text{eb}} \\ \text{fcn}(x,\beta), & x \in \mathcal{S}^+_{\text{eb}} \cup \mathcal{S}^0_{\text{eb}}. \end{cases} \tag{6}$$

In (6), the subfunction fcn is assumed to be a $\mathcal{C}^\infty$ function of (x,β). In addition, the global event-based parameter $\beta \in \mathcal{B}$ is used for $\theta(x) \geq \theta_{\text{eb}}$, whereas $\beta^\star \in \mathcal{B}$, referred to as the *nominal and global event-based parameter*, is employed for $\theta(x) < \theta_{\text{eb}}$. Assumption 4 will show how to choose the nominal parameter $\beta^\star$ to preserve the periodic orbit $\mathcal{O}$ for the closed-loop system. We remark that the event-based controllers of Section III-B updates the parameter from the nominal value $\beta^\star$ to β when state solutions intersect the event-based manifold $\mathcal{S}^0_{\text{eb}}$.

Assumption 3: ($\mathcal{C}^1$ Continuity): For every $(x,\beta) \in \mathcal{S}^0_{\text{eb}} \times \mathcal{B}$, $\text{fcn}(x,\beta)$ satisfies[2] (1) $\text{fcn}(x,\beta^\star) = \text{fcn}(x,\beta)$, (2) $\frac{\partial \text{fcn}}{\partial x}(x,\beta^\star) = \frac{\partial \text{fcn}}{\partial x}(x,\beta)$, and (3) $\frac{\partial \text{fcn}}{\partial \beta}(x,\beta^\star) = 0$ which in turn implies that the continuous-time feedback law Γ in (6) is $\mathcal{C}^1$ with respect to (x,β) on $\mathcal{X} \times \mathcal{B}$.

The evolution of the closed-loop system during the continuous-time phase can be described by the following $\mathcal{C}^1$, parameterized, and piecewise-defined vector field

$$\dot{x} = f^{\text{cl}}(x,\beta) := \begin{cases} f^{\text{cl}}_0(x,\beta^\star), & x \in \mathcal{S}^-_{\text{eb}} \\ f^{\text{cl}}_0(x,\beta), & x \in \mathcal{S}^+_{\text{eb}} \cup \mathcal{S}^0_{\text{eb}}, \end{cases} \tag{7}$$

where $f^{\text{cl}}_0(x,\beta) := f(x) + g(x)\,\text{fcn}(x,\beta)$. We refer to $f^{\text{cl}}_0(x,\beta^\star)$ and $f^{\text{cl}}_0(x,\beta)$ as the *pre-update* and *post-update closed-loop vector fields*, respectively, whose corresponding state spaces are given by $\mathcal{S}^-_{\text{eb}}$ and $\mathcal{S}^0_{\text{eb}} \cup \mathcal{S}^+_{\text{eb}}$. For later purposes, the unique solution of the closed-loop ODE $\dot{x} = f^{\text{cl}}(x,\beta)$ with the initial condition $x(0) = x_0$ is denoted by $x(t) = \varphi^f(t, x_0, \beta)$ for all $t \geq 0$ in the maximal interval of existence.

Assumption 4: (Nominal Event-Based Parameter): There exists a nominal and global parameter $\beta^\star \in \mathcal{B}$ such that $\varphi^f(t, \Delta(x^\star), \beta^\star) = \varphi^\star(t)$ for all $t \in [0, T^\star)$, where $\varphi^\star(t)$, $T^\star$, and $x^\star$ were already defined in Assumption 1. In particular, we assume that $\Gamma(\varphi^\star(t), \beta^\star) = u^\star(t)$ for all $t \in [0, T^\star)$.

B. Event-Based Controllers

This section presents a class of dynamic event-based controllers to exponentially/robustly stabilize the periodic orbit $\mathcal{O}$. This class of controllers takes the following *general* nonlinear form

$$\beta^+ = \pi(x^-, e^-) \tag{8}$$

$$e^+ = A_e\, e^- + \zeta(x^-), \tag{9}$$

in which the superscripts "$-$" and "$+$" denote the quantities corresponding to the pre- and post-update phases, respectively. Here, $e \in \mathbb{R}^l$ represents the *global event-based state variables* for some positive integer l. In addition, $\pi : \mathcal{X} \times \mathbb{R}^l \to \mathcal{B}$ denotes the *event-based controller*, assumed to be a $\mathcal{C}^1$ function of (x,e). The internal dynamics of the event-based controller are then given by (9) for which $A_e \in \mathbb{R}^{l\times l}$ and $\zeta : \mathcal{X} \to \mathbb{R}^l$ is a $\mathcal{C}^1$ function of x.

Assumption 5: (Fixed Point): Let us define the intersection of the desired orbit $\mathcal{O}$ and the event-based manifold $\mathcal{S}^0_{\text{eb}}$ as follows

$$\{x^\star_{\text{eb}}\} := \mathcal{O} \cap \mathcal{S}^0_{\text{eb}} = \{x_{\text{des}}(\theta_{\text{eb}})\}. \tag{10}$$

[2]Since for $\theta(x) < \theta_{\text{eb}}$, $\Gamma(x,\beta) = \text{fcn}(x,\beta^\star)$ and Γ is not a function of β, the condition $\frac{\partial \text{fcn}}{\partial \beta}(x,\beta^\star) = 0$ guarantees the $\mathcal{C}^1$ continuity of Γ with respect to β on $\mathcal{X} \times \mathcal{B}$.

The event-based controllers (8) and (9) are assumed to satisfy the conditions $\pi\left(x^\star_{\text{eb}}, 0\right) = \beta^\star$ and $\zeta\left(x^\star_{\text{eb}}\right) = 0$ to preserve the orbit for the closed-loop system.

C. Poincaré Return Map

This section presents the Poincaré return map for the closed-loop hybrid system and investigates the Jacobian linearization of the Poincaré map. Let us consider the following *augmented* and *double-phase closed-loop hybrid model*

$$\Sigma_a^{\text{cl},-}: \begin{cases} \begin{bmatrix} \dot{x} \\ \dot{\beta} \\ \dot{e} \end{bmatrix} = \begin{bmatrix} f_0^{\text{cl}}\left(x, \beta^\star\right) \\ 0 \\ 0 \end{bmatrix}, & x \in \mathcal{S}_{\text{eb}}^- \\ \begin{bmatrix} x^+ \\ \beta^+ \\ e^+ \end{bmatrix} = \begin{bmatrix} x^- \\ \pi\left(x^-, e^-\right) \\ A_e\, e^- + \zeta\left(x^-\right) \end{bmatrix}, & x^- \in \mathcal{S}_{\text{eb}}^0 \end{cases}$$

$$\Sigma_a^{\text{cl},+}: \begin{cases} \begin{bmatrix} \dot{x} \\ \dot{\beta} \\ \dot{e} \end{bmatrix} = \begin{bmatrix} f_0^{\text{cl}}\left(x, \beta\right) \\ 0 \\ 0 \end{bmatrix}, & x \in \left(\mathcal{S}_{\text{eb}}^0 \cup \mathcal{S}_{\text{eb}}^+\right) \setminus \mathcal{S} \\ \begin{bmatrix} x^+ \\ \beta^+ \\ e^+ \end{bmatrix} = \begin{bmatrix} \Delta\left(x^-\right) + d \\ \beta^\star \\ e^- \end{bmatrix}, & x^- \in \mathcal{S} \cap \left(\mathcal{S}_{\text{eb}}^0 \cup \mathcal{S}_{\text{eb}}^+\right), \end{cases} \tag{11}$$

in which the subscript "a" stands for the augmented model. During the pre-update phase of the hybrid system (11), the state space is given by $\mathcal{S}_{\text{eb}}^-$ and we define the *time-to-update* function $T^- : \mathcal{S}_{\text{eb}}^- \to \mathbb{R}_{>0}$ by $T^-\left(x_0\right) := \inf\left\{t > 0 \,|\, \varphi^f\left(t, x_0, \beta^\star\right) \in \mathcal{S}_{\text{eb}}^0\right\}$ as the first time at which the state solution of the system, i.e., $\varphi^f(t, x_0, \beta^\star)$, intersects the event-based manifold $\mathcal{S}_{\text{eb}}^0$. The *pre-update flow map* of the system can then be defined as $\mathcal{F}^- : \mathcal{S}_{\text{eb}}^- \to \mathcal{S}_{\text{eb}}^0$ by

$$\mathcal{F}^-\left(x_0\right) := \varphi^f\left(T^-\left(x_0\right), x_0, \beta^\star\right). \tag{12}$$

These definitions can be easily extended to the post-update phase for which the state space is given by $\mathcal{S}_{\text{eb}}^0 \cup \mathcal{S}_{\text{eb}}^+$. In particular, one can define the *time-to-impact* function $T^+ : \left(\mathcal{S}_{\text{eb}}^0 \cup \mathcal{S}_{\text{eb}}^+\right) \times \mathcal{B} \to \mathbb{R}_{>0}$ by $T^+\left(x_0, \beta\right) := \inf\left\{t > 0 \,|\, \varphi^f\left(t, x_0, \beta\right) \in \mathcal{S}\right\}$ as the first time at which the state solution $\varphi^f(t, x_0, \beta)$ intersects the switching manifold $\mathcal{S}$. The *post-update flow map* of the system is then defined as $\mathcal{F}^+ : \left(\mathcal{S}_{\text{eb}}^0 \cup \mathcal{S}_{\text{eb}}^+\right) \times \mathcal{B} \to \mathcal{S}$ by

$$\mathcal{F}^+\left(x_0, \beta\right) := \varphi^f\left(T^+\left(x_0, \beta\right), x_0, \beta\right). \tag{13}$$

Next we define the *parameterized Poincaré return map* as $P : \mathcal{S}_{\text{eb}}^0 \times \mathcal{B} \times \mathcal{D} \to \mathcal{S}_{\text{eb}}^0$ by the following composition rule

$$P\left(x, \beta, d\right) := \mathcal{F}^-\left(\Delta\left(\mathcal{F}^+\left(x, \beta\right)\right) + d\right) \tag{14}$$

to describe the evolution of the hybrid system (11) on the *augmented Poincaré section* $\mathcal{S}_{\text{eb}}^0 \times \mathbb{R}^l$ as follows

$$\hat{\mathcal{P}}_a: \begin{cases} \begin{bmatrix} x[k+1] \\ e[k+1] \end{bmatrix} = \begin{bmatrix} P\left(x[k], \pi\left(x[k], e[k]\right), d[k]\right) \\ A_e\, e[k] + \zeta\left(x[k]\right) \end{bmatrix} \\ k = 0, 1, \cdots \\ c[k] = z\left(x[k]\right). \end{cases} \tag{15}$$

Here, $\{d[k]\}_{k=0}^\infty$ and $\{c[k]\}_{k=0}^\infty$ represent the sequence of unknown exogenous input (i.e., disturbance) and output, respectively, for which $z(x)$ is assumed to be a $\mathcal{C}^1$ function. Motivated by designing a controller to minimize the effect of the disturbance input d on some control performances, we define the output function $c[k]$ on the Poincaré section (Section V will design $\mathcal{H}_2$- and $\mathcal{H}_\infty$-optimal controllers). For the case of bipedal walking, one can define $c[k]$ as the robot's center of mass (COM) velocity (see Section VII). According to the construction procedure in Assumptions 1-5, $(x^\star_{\text{eb}}, 0)$ is a *fixed point* for the system (15) in the absence of the disturbance input d. Linearization of the discrete-time system (15) around $(x, e, d) = (x^\star_{\text{eb}}, 0, 0)$ then results in the following system

$$\partial\hat{\mathcal{P}}_a: \begin{cases} \begin{bmatrix} \delta x[k+1] \\ \delta e[k+1] \end{bmatrix} = \underbrace{\begin{bmatrix} A_{11} & A_{12} \\ A_{21} & A_e \end{bmatrix}}_{=:A_{\text{cl}}} \begin{bmatrix} \delta x[k] \\ \delta e[k] \end{bmatrix} + \underbrace{\begin{bmatrix} E \\ 0 \end{bmatrix}}_{=:E_{\text{cl}}} d[k] \\ k = 0, 1, \cdots \\ \delta c[k] = \underbrace{\begin{bmatrix} C & 0 \end{bmatrix}}_{=:C_{\text{cl}}} \begin{bmatrix} \delta x[k] \\ \delta e[k] \end{bmatrix}, \end{cases} \tag{16}$$

in which $\delta x[k] := x[k] - x^\star_{\text{eb}}$, $\delta e[k] := e[k]$, $\delta c[k] := c[k] - c^\star_{\text{eb}}$, and $c^\star_{\text{eb}} := z\left(x^\star_{\text{eb}}\right)$. In particular,

$$A_{11} := A + B\,\frac{\partial \pi}{\partial x}\left(x^\star_{\text{eb}}, 0\right) \tag{17}$$

$$A_{12} := B\,\frac{\partial \pi}{\partial e}\left(x^\star_{\text{eb}}, 0\right) \tag{18}$$

$$A_{21} := \frac{\partial \zeta}{\partial x}\left(x^\star_{\text{eb}}\right), \tag{19}$$

where $A := \frac{\partial P}{\partial x}\left(x^\star_{\text{eb}}, \beta^\star, 0\right)$, $B := \frac{\partial P}{\partial \beta}\left(x^\star_{\text{eb}}, \beta^\star, 0\right)$, $E := \frac{\partial P}{\partial d}\left(x^\star_{\text{eb}}, \beta^\star, 0\right)$, and $C := \frac{\partial z}{\partial x}\left(x^\star_{\text{eb}}\right)$. In order to simplify the robustness analysis, we present the following lemma to connect the double-phase closed-loop hybrid system (11) to an equivalent single-phase hybrid system.

Lemma 1: (Single-Phase Closed-Loop Hybrid System): Suppose that Assumptions 1-5 are satisfied. Then, the following statements are correct.

1) $\hat{\mathcal{P}}_a$ is a Poincaré return map for the following *single-phase* closed-loop hybrid system

$$\hat{\Sigma}_a^{\text{cl}}: \begin{cases} \begin{bmatrix} \dot{x} \\ \dot{e} \end{bmatrix} = \begin{bmatrix} f_0^{\text{cl}}\left(x, \beta^\star\right) \\ 0 \end{bmatrix}, & x \in \mathcal{S}_{\text{eb}}^- \\ \begin{bmatrix} x^+ \\ e^+ \end{bmatrix} = \begin{bmatrix} \hat{\Delta}_x\left(x^-, e^-\right) + d \\ \hat{\Delta}_e\left(x^-, e^-\right) \end{bmatrix}, & x^- \in \mathcal{S}_{\text{eb}}^0, \end{cases} \tag{20}$$

   in which $\hat{\Delta}_x\left(x^-, e^-\right) := \Delta\left(\mathcal{F}^+\left(x^-, \pi\left(x^-, e^-\right)\right)\right)$ and $\hat{\Delta}_e\left(x^-, e^-\right) := A_e\, e^- + \zeta\left(x^-\right)$.
2) Let us decompose $\mathcal{O}$ as $\mathcal{O} = \mathcal{O}^- \cup \mathcal{O}^+$, where $\mathcal{O}^- := \mathcal{O} \cap \mathcal{S}_{\text{eb}}^-$ and $\mathcal{O}^+ := \mathcal{O} \cap \left(\mathcal{S}_{\text{eb}}^0 \cup \mathcal{S}_{\text{eb}}^+\right)$. Then, $\hat{\mathcal{O}}_a := \mathcal{O}^- \times \{0\} \subset \mathcal{S}_{\text{eb}}^- \times \mathbb{R}^l$ is an augmented period-one orbit for (20) in the absence of the disturbance input d that is transversal to the augmented guard $\mathcal{S}_{\text{eb}}^0 \times \mathbb{R}^l$.

Proof: From [23, Theorem 4.3, pp. 95], the proof is immediate. ■

D. ISS Property of the Periodic Orbit

This section addresses the ISS property of the augmented closed-loop hybrid system (20) with respect to the augmented orbit $\hat{\mathcal{O}}_a$. In order to make this notion precise, we present the following definition which is compatible with [52].

Definition 2 (Orbital ISS Property): The closed-loop hybrid system (20) has the local ISS property with respect to $\hat{\mathcal{O}}_a$ if there exit $\delta > 0$, a class $\mathcal{KL}$ function ρ, and a class $\mathcal{K}$ function α such that for every initial condition $x_a(0) := (x(0)^\top, e(0)^\top)^\top \in \mathcal{S}_{\text{eb}}^- \times \mathbb{R}^l$ with the property $\text{dist}(x_a(0), \hat{\mathcal{O}}_a) < \delta$ and the disturbance sequence input $\{d[k]\}_{k=0}^{\infty}$ with $d[k] \in \mathcal{N}_\delta(0) \subset \mathcal{D}$, $k \geq 0$, the state solution of the hybrid system (20), starting from the initial condition $x_a(0)$ and shown by $\hat{\varphi}_a(t)$, satisfies

$$\text{dist}\left(\hat{\varphi}_a(t), \hat{\mathcal{O}}_a\right) \leq \rho\left(\text{dist}\left(x_a(0), \hat{\mathcal{O}}_a\right), t\right) + \alpha\left(\|d\|_{l_\infty}\right), \tag{21}$$

for all $t \geq 0$.

The following theorem studies the orbital ISS property for the closed-loop hybrid system (20).

Theorem 1 (Orbital ISS Property): Suppose that Assumptions 1-5 are satisfied and $\hat{\mathcal{O}}_a$ is exponentially stable for $\hat{\Sigma}_a^{\text{cl}}$. Then, the closed-loop hybrid system (20) has the local ISS property with respect to $\hat{\mathcal{O}}_a$.

Proof: See Appendices A and B. ∎

Remark 2: Theorem 1 presents an upper bound for the distance of the state solutions to the orbit based on the ISS property. The result in (21) is different from that presented in [53]. In particular, [53] only studied the ISS property for the discrete-time system on the Poincaré section and did *not* relate it to the distance of the state solutions to the orbit.

IV. Class of Decentralized Two-level Controllers

The objective of this section is to propose a class of decentralized two-level controllers to exponentially/robustly stabilize the periodic orbit $\mathcal{O}$ for (1).

A. Interconnected Hybrid Subsystems

Motivated by the decentralized control design problem for a transpelvic amputee (the "human" part) walking with a prosthetic leg (the "robotic" part), we assume that the hybrid system (1) is composed of *two interconnected hybrid subsystems* Σ_1 and Σ_2. The *local state variables* and *local control inputs* for the subsystem Σ_i are represented by $x_i \in \mathcal{X}_i$ and $u_i \in \mathcal{U}_i$, respectively. In our notation, the subscript $i \in \{1, 2\}$ denotes the subsystem number. Furthermore, $\mathcal{X}_i \subset \mathbb{R}^{n_i}$ and $\mathcal{U}_i \subset \mathbb{R}^{m_i}$ are the *local state manifold* and *admissible set of local control inputs* for some positive integers n_i and m_i. Without loss of generality, we assume that the global state variables and global control inputs can be decomposed as $x = (x_1^\top, x_2^\top)^\top$ and $u = (u_1^\top, u_2^\top)^\top$. The continuous-time controllers, discrete-time controllers, and event-based parameters are also decomposed as $\Gamma = (\Gamma_1^\top, \Gamma_2^\top)^\top$, $\pi = (\pi_1^\top, \pi_2^\top)^\top$, and $\beta = (\beta_1^\top, \beta_2^\top)^\top$, respectively. In the proposed two-level control scheme, the decentralized controllers (continuous- and discrete-time) are assumed to have access to their own local measurements (i.e., local state variables x_i) as well as a subset of measurable global variables.

Definition 3 (Measurable Global Variables): Global variables are defined as quantities that are dependent on the global state vector $x = (x_1^\top, x_2^\top)^\top$. The global variable $\psi^{\text{ct}}(x) = \psi^{\text{ct}}(x_1, x_2)$ is said to be *measurable in continuous-time* for the subsystem Σ_i, $i \in \{1, 2\}$, if there are sensors to measure it along the solutions of Σ_i. The global variable $\psi^{\text{dt}}(x) = \psi^{\text{dt}}(x_1, x_2)$ is said to be *measurable in discrete-time* for the subsystem Σ_i, $i \in \{1, 2\}$, if it can be measured once per continuous-time phase when the solutions of Σ_i intersect the event-based manifold $\mathcal{S}_{\text{eb}}^0$.

Section VII will study continuous- and discrete-time measurable global variables for the case of bipedal walking. For the purpose of this paper, we make the following assumption.

Assumption 6: (Set of Measurable Global Variables): The set of continuous-time measurable global variables for the subsystem Σ_i, $i \in \{1, 2\}$, can be written in the following chain form

$$\Psi_i^{\text{ct}}(x) := \left(\psi_i^{\text{ct}\top}(x), \frac{\text{d}}{\text{d}t}\psi_i^{\text{ct}\top}(x), \cdots, \frac{\text{d}^{r-1}}{\text{d}t^{r-1}}\psi_i^{\text{ct}\top}(x)\right)^\top \in \mathbb{R}^{r\nu_i} \tag{22}$$

for some smooth and continuous-time measurable global variables $\psi_i^{\text{ct}}(x) \in \mathbb{R}^{\nu_i}$ and some positive integers $\nu_i \geq 1$. We further assume that the global variables $\psi_i^{\text{ct}}(x)$ have the relative degree r with respect to u. The set of discrete-time measurable global variables for the subsystem Σ_i, $i \in \{1, 2\}$ is directly formed as $\Psi_i^{\text{dt}}(x) := \psi_i^{\text{dt}}(x)$ for some $\mathcal{C}^1$ discrete-time measurable global variables $\psi_i^{\text{dt}}(x) \in \mathbb{R}^{\vartheta_i}$ and some positive integer $\vartheta_i \geq 1$.

Assumption 7: (Coordination of Controllers): The coordination of the cooperative subsystems is done through feeding back the phasing variable and its time-derivatives up to the order $(r-1)$ to the decentralized controllers[3]. In particular, the vector $\Theta(x)$, defined in (3), is assumed to be a *common* set of continuous-time measurable global variables for both subsystems Σ_1 and Σ_2.

B. Lower-Level Decentralized Continuous-Time Controllers

We present the class of parameterized decentralized continuous-time controllers $\Gamma_i : \mathcal{X}_i \times \mathbb{R}^r \times \mathbb{R}^{r\nu_i} \times \mathcal{B}_i \to \mathcal{U}_i$, $i \in \{1, 2\}$ by the following piecewise-defined policy

$$\Gamma_i\left(x_i, \Theta(x), \Psi_i^{\text{ct}}(x), \beta_i\right) := \begin{cases} \text{fcn}_i\left(x_i, \Theta, \Psi_i^{\text{ct}}, \beta_i^\star\right), & x \in \mathcal{S}_{\text{eb}}^- \\ \text{fcn}_i\left(x_i, \Theta, \Psi_i^{\text{ct}}, \beta_i\right), & x \in \mathcal{S}_{\text{eb}}^+ \cup \mathcal{S}_{\text{eb}}^0, \end{cases} \tag{23}$$

where the subfunctions fcn_i, $i \in \{1, 2\}$ are assumed to be $\mathcal{C}^\infty$ functions of $(x_i, \Theta, \Psi_i^{\text{ct}}, \beta_i)$. The proposed continuous-time controllers in (23) have access to (1) the local state variables x_i, (2) the sequence of the phasing variable derivatives $\Theta(x)$, (3) the set of continuous-time measurable global variables $\Psi_i^{\text{ct}}(x)$, and (4) the local event-based parameters β_i. We also

[3]The need for this assumption will be clarified in Proposition 1, in which the decentralized I-O linearizing controllers require the measurement of the local output functions as well as their time derivatives up to the order $(r-1)$.

note that the decentralized continuous-time laws in (23) are dependent on *two* different sets of continuous-time measurable global variables. In particular according to Assumption 7, $\Theta(x)$ is a common set of measurable global variables for both subsystems to coordinate the action of decentralized controllers. In addition, each decentralized controller has access to its own set of measurable global variables $\Psi_i^{\text{ct}}(x)$ to improve some control performances such as robust stability. This will be clarified with more details for the case of bipedal walking in Section VII.

C. Decentralized Output Regulators

In this section, we address an important family of decentralized continuous-time controllers presented in (23) to zero a set of local output functions. We show that this family of decentralized controllers satisfies Assumptions 3 and 4. For this purpose, let us define a parameterized local output function $y_i : \mathcal{X}_i \times \mathbb{R}^r \times \mathbb{R}^{r\nu_i} \times \mathcal{B}_i \to \mathbb{R}^{m_i}$ for the subsystem $\Sigma_i, i \in \{1,2\}$ as follows

$$\begin{aligned} y_i\left(x_i, \Theta(x), \Psi_i^{\text{ct}}(x), \beta_i\right) := & H_i\left(x_i - x_{\text{des},i}(\theta)\right) \\ & + \hat{H}_i\left(\psi_i^c - \psi_{\text{des},i}^{\text{ct}}(\theta)\right) \\ & - y_{\text{sta},i}\left(\theta, \beta_i\right) \end{aligned} \tag{24}$$

in which $\dim(y_i) = \dim(u_i) = m_i$, and $H_i \in \mathbb{R}^{m_i \times n_i}$ and $\hat{H}_i \in \mathbb{R}^{m_i \times \nu_i}$ represent the full-rank local output matrices. Here, $\psi_{\text{des},i}^{\text{ct}}(\theta) \in \mathbb{R}^{\nu_i}$ denotes the desired evolution of the continuous-time global variables $\psi_i^{\text{ct}}(x)$ on the periodic orbit $\mathcal{O}$ expressed in terms of the phasing variable $\theta(x)$. The first two terms in (24) vanish on the desired orbit $\mathcal{O}$. The *stabilizing local output* $y_{\text{sta},i} : \mathbb{R} \times \mathcal{B}_i \to \mathbb{R}^{m_i}$ is then defined by the following piecewise rule

$$y_{\text{sta},i}\left(\theta, \beta_i\right) := \begin{cases} 0, & \theta < \theta_{\text{eb}} \\ b_i\left(\theta, \beta_i\right), & \theta \geq \theta_{\text{eb}} \end{cases} \tag{25}$$

that is zero during the *pre-update phase* (i.e., $\theta(x) < \theta_{\text{eb}}$) and equals $b_i\left(\theta, \beta_i\right)$ during the *post-update phase* (i.e., $\theta(x) \geq \theta_{\text{eb}}$). Here, the subfunction $b_i : \mathbb{R} \times \mathcal{B}_i \to \mathbb{R}^{m_i}$ is assumed to be a $\mathcal{C}^\infty$ function with respect to (θ, β_i) satisfying the following two conditions:

C1) There exists $\beta_i^\star \in \mathcal{B}_i$ such that $b_i(\theta, \beta_i^\star) \equiv 0$, and
C2) $b_i(\theta_{\text{eb}}, \beta_i) = \frac{\partial b_i}{\partial \theta}(\theta_{\text{eb}}, \beta_i) = \cdots = \frac{\partial^r b_i}{\partial \theta^r}(\theta_{\text{eb}}, \beta_i) = 0$ for all $\beta_i \in \mathcal{B}_i$.

The following proposition presents a family of decentralized continuous-time controllers to zero the output functions (24) and then verifies Assumptions 3 and 4 for this family.

Proposition 1: (Decentralized Output Zeroing Controllers): Consider the local output functions $y_i, i \in \{1,2\}$, in (24) and assume that Assumptions 1, 2, 6, and 7 are met. Suppose further Conditions C1 and C2 are satisfied and the output functions have the relative degree r with respect to the control input u. Let us define the following family of decentralized output zeroing controllers

$$\Gamma_i = u_i^\star(\theta) - R_i^{-1}\left(x_i\right)\left(\sum_{j=0}^{r-1} \kappa_j\, y_i^{(j)}\right), \tag{26}$$

where $R_i(x_i) \in \mathbb{R}^{m_i \times m_i}$ is a smooth and invertible local decoupling matrix, $y_i^{(j)} := \frac{\mathrm{d}^j y_i}{\mathrm{d}t^j}$ for $i \in \{1,2\}$ and $0 \leq j \leq r-1$, and constants κ_j, $0 \leq j \leq r-1$ are chosen such that the monic polynomial $\lambda^r + \kappa_{r-1}\lambda^{r-1} + \cdots + \kappa_1\lambda + \kappa_0$ becomes Hurwitz. Then, Assumptions 3 and 4 are satisfied. Furthermore, $\Gamma_i, i \in \{1,2\}$ in (26) are functions of $(x_i, \Theta, \Psi_i^{\text{ct}}, \beta_i)$.

Proof: From Condition C1, the local output function $y_i(x_i, \Theta(x), \Psi_i^{\text{ct}}(x), \beta_i)$ vanishes[4] on the orbit $\mathcal{O}$ for $\beta_i = \beta_i^\star$. Condition C2 together with Assumptions 2 and 6 makes the output function $y_i(x_i, \Theta(x), \Psi_i^{\text{ct}}(x), \beta_i)$ r-times continuously differentiable with respect to (x, β_i). Hence, the decentralized continuous-time controllers $\Gamma_i, i \in \{1,2\}$ in (26) are $\mathcal{C}^1$ with respect to (x, β_i) and satisfy Assumption 3. Furthermore, since the local output functions and their consecutive time-derivatives up to the order $(r-1)$ are identically zero on the orbit $\mathcal{O}$ for $\beta = \beta^\star$, Assumption 4 is met. According to Assumptions 2 and 6, $y_i^{(j)}$, for every $i \in \{1,2\}$ and $0 \leq j \leq r-1$, is only a function of $(x_i, \Theta, \Psi_i^{\text{ct}}, \beta_i)$. Consequently, the feedback laws Γ_i in (26) are indeed functions of $(x_i, \Theta, \Psi_i^{\text{ct}}, \beta_i)$. ■

D. Higher-Level Decentralized Event-Based Controllers

Our proposed class of event-based controllers takes the following *general* nonlinear form

$$\beta_i^+ = \pi_i\left(x_i^-, \Psi_i^{\text{ct}}(x^-), \Psi_i^{\text{dt}}(x^-), e_i^-\right) \tag{27}$$

$$e_i^+ = A_{e,i}\, e_i^- + \zeta_i\left(x_i^-, \Psi_i^{\text{ct}}(x^-), \Psi_i^{\text{dt}}(x^-)\right). \tag{28}$$

In (27) and (28), $e_i \in \mathbb{R}^{l_i}$ represents the *local event-based state variables* for some positive integer l_i. In addition, $\pi_i : \mathcal{X}_i \times \mathbb{R}^{r\nu_i} \times \mathbb{R}^{\vartheta_i} \times \mathbb{R}^{l_i} \to \mathcal{B}_i$, $i \in \{1,2\}$ denotes the *decentralized event-based controller* for Σ_i, assumed to be a $\mathcal{C}^1$ function of $(x_i, \Psi_i^{\text{ct}}, \Psi_i^{\text{dt}}, e_i)$. The internal dynamics of the event-based controller are then given by (28) for which $A_{e,i} \in \mathbb{R}^{l_i \times l_i}$ and $\zeta_i : \mathcal{X}_i \times \mathbb{R}^{r\nu_i} \times \mathbb{R}^{\vartheta_i} \to \mathbb{R}^{l_i}$ is a $\mathcal{C}^1$ function of $(x_i, \Psi_i^{\text{ct}}, \Psi_i^{\text{dt}})$. Unlike the decentralized continuous-time controllers that only depend on the set of continuous-time measurable global variables, the decentralized event-based controllers are assumed to depend on both sets of continuous- and discrete-time measurable global variables $\Psi_i^{\text{ct}}(x)$ and $\Psi_i^{\text{dt}}(x)$.

For the rest of this paper, we will employ the following affine decentralized event-based controllers that satisfy Assumption 5:

$$\pi_i := -K_i\left(x_i - x_{\text{eb},i}^\star\right) - \hat{K}_i\left(\Psi_i(x) - \Psi_i^\star\right) - \tilde{K}_i\, e_i + \beta_i^\star \tag{29}$$

$$\zeta_i := \quad W_i\left(x_i - x_{\text{eb},i}^\star\right) + \hat{W}_i\left(\Psi_i(x) - \Psi_i^\star\right), \tag{30}$$

where $\Psi_i(x) := (\Psi_i^{\text{ct}\top}, \Psi_i^{\text{dt}\top})^\top \in \mathbb{R}^{r\nu_i + \vartheta_i}$, $\Psi_i^\star := \Psi_i(x_{\text{eb}}^\star)$, $W_i \in \mathbb{R}^{l_i \times n_i}$ and $\hat{W}_i \in \mathbb{R}^{l_i \times (r\nu_i + \vartheta_i)}$. Furthermore, $K_i \in \mathbb{R}^{p_i \times n_i}$, $\hat{K}_i \in \mathbb{R}^{p_i \times (r\nu_i + \vartheta_i)}$, and $\tilde{K}_i \in \mathbb{R}^{p_i \times l_i}$ represent the *local event-based gains* to be determined in Section V. Using

[4]For $\beta_i \neq \beta_i^\star$, the local output function $y_i(x_i, \Theta(x), \psi_i^{\text{ct}}(x), \beta_i)$ is zero on $\mathcal{O}$ for $\theta(x) \leq \theta_{\text{eb}}$. However, it is not zero on $\mathcal{O}$ for $\theta(x) > \theta_{\text{eb}}$.

(29) and (30), one can show that

$$\frac{\partial \pi}{\partial x}(x^\star_{\text{eb}},0) = -\begin{bmatrix} K_1 & 0 \\ 0 & K_2 \end{bmatrix} - \begin{bmatrix} \hat{K}_1 & 0 \\ 0 & \hat{K}_2 \end{bmatrix} \Upsilon \tag{31}$$

$$\frac{\partial \pi}{\partial e}(x^\star_{\text{eb}},0) = -\begin{bmatrix} \tilde{K}_1 & 0 \\ 0 & \tilde{K}_2 \end{bmatrix} \tag{32}$$

$$\frac{\partial \zeta}{\partial x}(x^\star_{\text{eb}}) = \begin{bmatrix} W_1 & 0 \\ 0 & W_2 \end{bmatrix} + \begin{bmatrix} \hat{W}_1 & 0 \\ 0 & \hat{W}_2 \end{bmatrix} \Upsilon, \tag{33}$$

where $\Upsilon := \frac{\partial \Psi}{\partial x}(x^\star_{\text{eb}})$, $\Psi(x) := (\Psi_1^\top, \Psi_2^\top)^\top$, $e = (e_1^\top, e_2^\top)^\top$, and $\zeta = (\zeta_1^\top, \zeta_2^\top)^\top$

V. Robust Stabilization Problem

This section addresses the robust stabilization problem of the hybrid periodic orbit $\mathcal{O}$ based on the Poincaré sections analysis and matrix inequalities. In order to minimize the effect of the disturbance sequence $\{d[k]\}_{k=0}^{\infty}$ on some control performances, we consider the $\mathcal{H}_2$ and $\mathcal{H}_\infty$ decentralized event-based control design problems. In particular, we present a BMI optimization framework to solve for the following problems.

Problem 1: ($\mathcal{H}_2$ Control Problem): The $\mathcal{H}_2$ control problem of parameter γ consists of finding the hextuple of local controller gains $(K_1, K_2, \hat{K}_1, \hat{K}_2, \tilde{K}_1, \tilde{K}_2)$ such that

1) $\mathcal{O}$ is exponentially stable for (11), and
2) the $\mathcal{H}_2$-norm of the transfer matrix T_{dc}, relating the disturbance input $d[k]$ to the controlled outputs $\delta c[k]$ in (16), becomes less than $\sqrt{\gamma}$, that is, $\|T_{dc}\|_{\mathcal{H}_2} < \sqrt{\gamma}$.

Problem 2: ($\mathcal{H}_\infty$ Control Problem): The $\mathcal{H}_\infty$ control problem of parameter γ consists of finding the hextuple of local controller gains $(K_1, K_2, \hat{K}_1, \hat{K}_2, \tilde{K}_1, \tilde{K}_2)$ such that

1) $\mathcal{O}$ is exponentially stable for (11), and
2) the $\mathcal{H}_\infty$ norm of the transfer matrix T_{dc} in (16), is less than γ, that is, $\|T_{dc}\|_{\mathcal{H}_\infty} < \gamma$.

Although many problems in control theory can be modeled using LMIs and solved using convex semidefinite programming, even more problems turn out to be non-convex. One of the most important problems in control theory is the design of static output feedback that is a non-convex semidefinite program [54], [55]. According to the structural controller constraint in A_{11} and A_{12} (see (17), (18), (31), and (32)), the problem of designing the hextuple $(K_1, K_2, \hat{K}_1, \hat{K}_2, \tilde{K}_1, \tilde{K}_2)$ cannot be handled using the LMI formulations of [20], [46]. In particular, the problem is a non-convex semidefinite program. In order to design optimal decentralized event-based controllers, the following proposition presents a BMI optimization framework based on the results of [46] and [56].

Proposition 2: (Optimal Decentralized Event-Based Control Design): Suppose that Assumptions 1-7 hold and let $w_0 > 0$, $w_1 > 0$, $w_2 > 0$, and $w_3 > 0$ be weighting factors. Then, the following statements are correct.

1) *($\mathcal{H}_2$-Optimal Decentralized Event-Based Control):* Assume that the following BMI optimization problem is feasible[5]:

$$\min_{\chi} \quad w_0\,\mu + w_1 \sum_{i=1}^{2} \eta_i + w_2 \sum_{i=1}^{2} \hat{\eta}_i + w_3 \sum_{i=1}^{2} \tilde{\eta}_i \tag{34}$$

$$\text{s.t.} \quad \begin{bmatrix} Q & A_{\text{cl}}\,Q & E_{\text{cl}} \\ \star & Q & 0 \\ \star & \star & I \end{bmatrix} > 0 \tag{35}$$

$$\begin{bmatrix} Z & C_{\text{cl}}\,Q \\ \star & Q \end{bmatrix} > 0 \tag{36}$$

$$\begin{bmatrix} I & \text{vec}(K_i) \\ \star & \eta_i \end{bmatrix} > 0, \quad i \in \{1,2\} \tag{37}$$

$$\begin{bmatrix} I & \text{vec}(\hat{K}_i) \\ \star & \hat{\eta}_i \end{bmatrix} > 0, \quad i \in \{1,2\} \tag{38}$$

$$\begin{bmatrix} I & \text{vec}(\tilde{K}_i) \\ \star & \tilde{\eta}_i \end{bmatrix} > 0, \quad i \in \{1,2\} \tag{39}$$

$$\text{trace}\,(Z) < \mu, \tag{40}$$

in which χ represents the $\mathcal{H}_2$ problem decision variables consisting of $Q = Q^\top$, $Z = Z^\top$, μ, K_i, $\hat{K}_i$, $\tilde{K}_i$, η_i, $\hat{\eta}_i$, and $\tilde{\eta}_i$ for $i \in \{1,2\}$. Then, $\mathcal{O}$ is exponentially stable for (11) and $\|T_{dc}\|_{\mathcal{H}_2} < \sqrt{\mu}$.

2) *($\mathcal{H}_\infty$-Optimal Decentralized Event-Based Control):* Assume that the following BMI optimization problem is feasible:

$$\min_{\chi} \quad w_0\,\mu + w_1 \sum_{i=1}^{2} \eta_i + w_2 \sum_{i=1}^{2} \hat{\eta}_i + w_3 \sum_{i=1}^{2} \tilde{\eta}_i \tag{41}$$

$$\text{s.t.} \quad \begin{bmatrix} -Q & Q\,A_{\text{cl}} & Q\,E_{\text{cl}} & 0 \\ \star & -Q & 0 & C_{\text{cl}}^\top \\ \star & \star & -\mu I & 0 \\ \star & \star & \star & -I \end{bmatrix} < 0 \tag{42}$$

$$\begin{bmatrix} I & \text{vec}(K_i) \\ \star & \eta_i \end{bmatrix} > 0, \quad i \in \{1,2\} \tag{43}$$

$$\begin{bmatrix} I & \text{vec}(\hat{K}_i) \\ \star & \hat{\eta}_i \end{bmatrix} > 0, \quad i \in \{1,2\} \tag{44}$$

$$\begin{bmatrix} I & \text{vec}(\tilde{K}_i) \\ \star & \tilde{\eta}_i \end{bmatrix} > 0, \quad i \in \{1,2\}, \tag{45}$$

in which χ represents the $\mathcal{H}_\infty$ problem decision variables consisting of $Q = Q^\top$, μ, K_i, $\hat{K}_i$, $\tilde{K}_i$, η_i, $\hat{\eta}_i$, and $\tilde{\eta}_i$ for $i \in \{1,2\}$. Then, $\mathcal{O}$ is exponentially stable for (11) and $\|T_{dc}\|_{\mathcal{H}_\infty} < \sqrt{\mu}$.

Proof: See Appendix C. ∎

In Proposition 2, (35) and (42) represent BMIs, whereas (36)-(40) and (43)-(45) denote LMIs in terms of the decision variables χ. According to the proof of Proposition 2, η_i, $\hat{\eta}_i$, and $\tilde{\eta}_i$ represent dynamic upper bounds for the Frobenius norm of the gain matrices K_i, $\hat{K}_i$, and $\tilde{K}_i$, respectively. The cost functions (34) and (41) then consist of a linear combination of μ (i.e., $\mathcal{H}_2$ and $\mathcal{H}_\infty$ parameters) and dynamic upper bounds η_i,

[5] $\star$ in the block (i,j) stands for the transpose of the block (j,i).

$\hat{\eta}_i$, and $\tilde{\eta}_i$ as a tradeoff between improving μ and minimizing the norms of the local gain matrices.

VI. Computation of the Jacobian Matrices

The objective of this section is to present a numerical approach to compute the Jacobian matrices (A, B, E) from (16)-(18) based on the continuous- and discrete-time dynamics of the closed-loop hybrid model (11).

Theorem 2: (Jacobian Matrices of the Poincaré Map): Suppose that Assumptions 1-5 are met. Let $\varphi^{f\star}(t)$ for $t \in [0, T^\star]$ denote the solution of the closed-loop ODE $\dot{x} = f^{\mathrm{cl}}(x, \beta^\star)$ with the initial condition $x(0) = \Delta(x^\star)$. Define the sensitivity trajectory matrices $\Phi_x^-(t)$, $\Phi_x^+(t)$, and $\Phi_\beta^+(t)$ using the following variational equations

$$\dot{\Phi}_x^-(t) = \frac{\partial f_0^{\mathrm{cl}}}{\partial x}\left(\varphi^{f\star}(t), \beta^\star\right)\Phi_x^-(t), \quad 0 \le t \le T^{-\star}$$
$$\dot{\Phi}_x^+(t) = \frac{\partial f_0^{\mathrm{cl}}}{\partial x}\left(\varphi^{f\star}(t), \beta^\star\right)\Phi_x^+(t), \quad T^{-\star} \le t \le T^\star$$
$$\dot{\Phi}_\beta^+(t) = \frac{\partial f_0^{\mathrm{cl}}}{\partial x}\left(\varphi^{f\star}(t), \beta^\star\right)\Phi_\beta^+(t) + \frac{\partial f_0^{\mathrm{cl}}}{\partial \beta}\left(\varphi^{f\star}(t), \beta^\star\right), \quad T^{-\star} \le t \le T^\star,$$

with the initial conditions $\Phi_x^-(0) = I$, $\Phi_x^+(T^{-\star}) = I$, and $\Phi_\beta^+(T^{-\star}) = 0$, in which $T^{-\star} := T^-(\Delta(x^\star))$. Then, the Poincaré map P, defined in (14), is $\mathcal{C}^1$ with respect to (x, β, d) on an open neighborhood of $(x_{\mathrm{eb}}^\star, \beta^\star, 0)$. Furthermore, the Jacobian matrices can be computed numerically as follows:

$$A = \Pi^-\,\Phi_x^-\left(T^{-\star}\right) D\,\Pi^+\,\Phi_x^+\left(T^\star\right) \tag{46}$$
$$B = \Pi^-\,\Phi_x^-\left(T^{-\star}\right) D\,\Pi^+\,\Phi_\beta^+\left(T^\star\right) \tag{47}$$
$$E = \Pi^-\,\Phi_x^-\left(T^{-\star}\right), \tag{48}$$

in which $D := \frac{\partial \Delta}{\partial x}(x^\star)$, and Π^- and Π^+ are the pre- and post-update saltation matrices defined as $\Pi^- := I - \frac{f_0^{\mathrm{cl}}(x_{\mathrm{eb}}^\star, \beta^\star)\frac{\partial \theta}{\partial x}(x_{\mathrm{eb}}^\star)}{\frac{\partial \theta}{\partial x}\left(x_{\mathrm{eb}}^\star\right) f_0^{\mathrm{cl}}\left(x_{\mathrm{eb}}^\star, \beta^\star\right)}$ and $\Pi^+ := I - \frac{f_0^{\mathrm{cl}}(x^\star, \beta^\star)\frac{\partial s}{\partial x}(x^\star)}{\frac{\partial s}{\partial x}(x^\star) f_0^{\mathrm{cl}}(x^\star, \beta^\star)}$.

Proof: See Appendix D. ∎

VII. Application to 3D Bipedal Walking

This section employs the proposed decentralized two-level control strategy to robustly stabilize a walking gait of an underactuated 3D bipedal robot.

A. Underactuated 3D Bipedal Model

The biped model forms a tree structure consisting of a torso and two identical legs[6] terminating at point feet (see Fig. 1). Each leg of the robot includes three actuated DOFs: a two-DOF hip (ball) joint with roll and pitch motions plus a one-DOF knee joint. During the single support phase, the robot has 9 DOFs, including 6 actuated DOFs of two legs and 3 unactuated DOFs corresponding to the absolute orientation of the torso link with respect to the world frame. To describe the absolute orientation, a frame is attached to the bottom of the torso link with the y-axis being in the direction of walking and the z-axis being upward. The orientation of the torso frame with respect to the world frame is then described by three Euler angles, referred to as the *yaw*, *roll*, and *pitch* angles. The kinematic and dynamic parameter values for the links are taken according to those reported in [57] for a 3D human model. The state vector of the mechanical system is taken as $x := (q^\top, \dot{q}^\top)^\top \in \mathcal{X} \subset \mathbb{R}^{18}$, in which q and $\dot{q}$ denote the generalized coordinates and velocity vectors, respectively. The control input is also shown by $u \in \mathcal{U} \subset \mathbb{R}^6$ to represent the motor torques applied at the actuated joints. Using [23, Theorem 4.3] and [58], one can present a single-phase hybrid model of walking as (1). The desired periodic walking gait $\mathcal{O}$ is designed using the motion planning algorithm of [13] for walking at the speed of 0.6 (m/s) with the cost of mechanical transport CMT = 0.07[7].

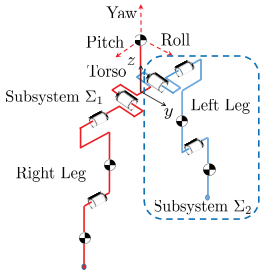

Fig. 1: The structure of the autonomous 3D bipedal robot [43]. The model has 9 DOFs with 3 unactuated Euler angles and 6 actuated revolute joints. Subsystems Σ_1 (human part) and Σ_2 (prosthetic part) with the corresponding DOFs have been shown in the figure.

B. Decentralization Scheme

As shown in Fig 1, the human and prosthetic leg subsystems are denoted by Σ_1 and Σ_2, respectively. The prosthetic subsystem Σ_2 includes the 3 DOFs of the left leg with the corresponding 3 actuators, whereas the human subsystem Σ_1 consists of the rest of the model, including the torso and right leg with 6 DOFs and 3 actuators. According to this decentralization scheme, the local state variables $x_1 \in \mathcal{X}_1 \subset \mathbb{R}^{12}$ consist of the corresponding shape variables and global orientation of the human part (assumed to come from the vestibular system). In particular, $x_1 = (q_1^\top, \dot{q}_1^\top)^\top$, in which $q_1 \in \mathbb{R}^6$ and $\dot{q}_1 \in \mathbb{R}^6$ denote the generalized position and velocity vectors for Σ_1, respectively. However, the local state variables $x_2 \in \mathcal{X}_2 \subset \mathbb{R}^6$ only include the shape variables for the prosthetic leg, i.e., $x_2 = (q_2^\top, \dot{q}_2^\top)^\top$, where $q_2 \in \mathbb{R}^3$ and $\dot{q}_2 \in \mathbb{R}^3$ represent the generalized position and velocity vectors for the left leg. In addition, $\dim(u_1) = \dim(u_2) = 3$.

In order to measure orientation for the prosthetic leg controller, we make use of two inertial measurement units (IMUs) attached to the thigh links: one on the human thigh and the other on the prosthetic thigh. The continuous-time global variables for Σ_2 (i.e., $\psi_2^{\mathrm{ct}}(x)$) are defined as the yaw and roll angles of these two IMUs, where relative degree $r = 2$ according to

[6] We suppose that the robotic and human legs have the same kinematic and dynamic parameters. This simplifies the trajectory planning process. However, our proposed stabilization approach and Assumption 1 do *not* require symmetry in the periodic orbit design. If the orbit does not have the left-right symmetry, the hybrid model of walking consists of two continuous-time phases. Then, one can apply [23, Theorem 4.3] to connect the double-phase model of walking into the single-phase model of (1).

[7] We consider the unilateral constraints to design the desired gait.

the second-order nature of the dynamics. The IMU pitch angle will be used to measure the phasing variable in $\Theta(x)$. The set of continuous-time measurable global variables for the prosthetic leg is taken as $\Psi_2^{\text{ct}}(x) := (\psi_2^{\text{ct}\top}(x), \dot{\psi}_2^{\text{ct}\top}(x))^\top \in \mathbb{R}^8$, in which $\dot{\psi}_2^{\text{ct}}(x)$ denotes the rate change of the Euler angles. One can also make use of the IMU feedback to estimate the linear velocity of a point on the biped (e.g., [59]), so the discrete-time measurable global variables $\Psi_2^{\text{dt}}(x)$ are assumed to be the x- and y-components of the prosthetic hip linear velocity measured at $\mathcal{S}_{\text{eb}}^0$. Since the global orientation for Σ_1 is implicitly included in the local state variables x_1 and the human controller does not have access to the IMU data, we can take the set of measurable global variables for Σ_1 as an empty set, i.e., $\Psi_1(x) = \emptyset$. This satisfies Assumption 6. Assumption 7 is not restrictive for models of bipedal walking. In particular, we define the phasing variable based on the absolute stance hip angle in the sagittal plane [43]. This angle θ and its first-order time-derivative $\dot{\theta}$, i.e., $\Theta(x) := (\theta(x), \dot{\theta}(x))^\top \in \mathbb{R}^2$, are measurable for the prosthetic leg subsystem (i.e., Σ_2) by the IMUs attached to the thigh links. It is further reasonable to assume that $\Theta(x)$ is available to the human part (i.e., subsystem Σ_1) through proprioception.

C. Decentralized Two-level Controllers

Mathematical models for the decentralized controller of the human part are not known. However, for the purpose of this paper, we assume that the decentralized controller for the human part is a *phase-dependent* nonlinear controller in a similar manner to [41], [43], [44]. Evidence suggests that the phase-dependent models can reasonably predict human joint behavior even across perturbations [45]. Consequently, we study the following decentralized two-level feedback control structure for underactuated 3D bipedal walking

$$u_1 = \Gamma_1\left(x_1, \Theta(x)\right) \tag{49}$$

$$u_2 = \Gamma_2\left(x_2, \Theta(x), \Psi_2^{\text{ct}}(x), \beta_2\right) \tag{50}$$

$$\beta_2^+ = \pi_2\left(x_2^-, \Psi_2^{\text{ct}}(x^-), \Psi_2^{\text{dt}}(x^-), e_2^-\right) \tag{51}$$

$$e_2^+ = e_2^- + \zeta_2\left(x_2^-, \Psi_2^{\text{ct}}(x^-), \Psi_2^{\text{dt}}(x^-)\right), \tag{52}$$

in which the internal dynamics of the decentralized event-based controller have been taken as a discrete-time integrator to reject step-like disturbances, i.e., $A_{e,2} = I$. In (49), the decentralized continuous-time controller for the human part $\Gamma_1(x_1, \Theta(x))$ is a phase-dependent nonlinear feedback law that does not have access to the data from the IMUs (i.e., $\Psi_1(x) = \emptyset$). In addition, we do *not* make use of any event-based controller for the human part. This has several consequences. First, we can use/adapt a fixed structure (i.e., no event-based action) for the human part decentralized controller that is known (e.g., through intuition or motion capture studies). Second, we can search for $\mathcal{H}_2$- and $\mathcal{H}_\infty$-optimal decentralized event-based controllers for the prosthesis while using the fixed structure for the decentralized controller of the human part.

D. Application to Virtual Constraints

Virtual constraints are defined as holonomic output functions $y(x)$ for continuous-time portions of hybrid models of walking to coordinate the links of bipedal robots within a stride [2], [3], [10], [27], [39], [40], [60]–[64]. Virtual constraints are typically enforced (i.e., $y \equiv 0$) by *centralized* I-O linearizing feedback laws [65] and have been numerically and experimentally validated for stable 2D and 3D underactuated bipedal robots [13], [27], [60], [62], [66], [67] and exoskeletons [42].

The objective of this section is to apply the analytical results of the paper to design $\mathcal{H}_2$- and $\mathcal{H}_\infty$-optimal decentralized event-based controllers for the prosthesis while the continuous-time controllers Γ_1 and Γ_2 in (49) and (50) take the form of (26) to enforce decentralized virtual constraints. In this paper, the decentralized virtual constraints are defined as (24). We only remark that they need to be holonomic quantities, and hence, one would need to replace x_i and $x_{\text{des},i}(\theta)$ in (24) with the local configuration variables q_i and corresponding desired evolution $q_{\text{des},i}(\theta)$. In particular, $y_1\left(x_1, \Theta(x)\right) := H_1(q_1 - q_{\text{des},1}(\theta))$ and $y_2\left(x_2, \Theta(x), \psi_2^{\text{ct}}(x), \beta_2\right) := H_2(q_2 - q_{\text{des},2}(\theta)) + \hat{H}_2(\psi_2^{\text{ct}}(q) - \psi_{\text{des},2}^{\text{ct}}(\theta)) - y_{\text{sta},2}\left(\theta, \beta_2\right)$, where $H_1 \in \mathbb{R}^{3\times 6}$, $H_2 \in \mathbb{R}^{3\times 3}$, and $\hat{H}_2 \in \mathbb{R}^{3\times 4}$ are output matrices [we note that $\hat{H}_1 = 0$ and $y_{\text{sta},1} \equiv 0$ to get the structure of (49)]. The stabilizing term $y_{\text{sta},2}\left(\theta, \beta_2\right) \in \mathbb{R}^3$ is then chosen as (25), in which $b_2(\theta, \beta_2) \in \mathbb{R}^3$ is a third-order parameterized polynomial given by $b_2\left(\theta, \beta_2\right) := H_2\, \beta_2 \left(\frac{\theta - \theta_{\text{eb}}}{\theta_{\max} - \theta_{\text{eb}}}\right)^3$. Here, $\beta_2 \in \mathcal{B}_2 \subset \mathbb{R}^3$ represents the event-based parameters for the subsystem Σ_2. In order to satisfy condition C1, we take the nominal event-based parameters as $\beta_2^\star = 0$ (Assumption 4). Furthermore, this choice satisfies condition C2 and makes the decentralized output zeroing controller for the prosthetic leg $\mathcal{C}^1$ with respect to x (Assumption 3). The lower-dimensional decoupling matrices in (26) are also taken as constant matrices, which reduces the decentralized continuous-time controllers Γ_1 and Γ_2 into a set of simple *PD controllers*.

We note that robust stability is achieved by the choice of the output functions and decentralized event-based controller. The output matrices H_1, H_2, and $\hat{H}_2$ are designed using the optimization algorithm of [43] so that the periodic gait $\mathcal{O}$ becomes exponentially stable in the absence of the event-based controller. We remark that even if the periodic orbit is not exponentially stable with the action of the continuous-time controllers, the optimal decentralized event-based controllers of Proposition 2 can make it exponentially stable. However, to increase the robustness of the orbit, we prefer to stabilize the gait with the continuous-time controllers (i.e., inner loop). The $\mathcal{H}_2$- and $\mathcal{H}_\infty$-optimal decentralized event-based controllers for Σ_2 then minimize the effect of contact model uncertainties on the walking gait (i.e., outer loop).

E. PENBMI Solver and Numerical Results

Unlike LMIs that are being used for centralized event-based controller design [20], BMIs are non-convex and NP-hard problems. However, PENBMI is a general-purpose solver that guarantees the convergence to a local optimal point satisfying the Karush Kuhn Tucker optimality conditions [68]. To solve the BMI optimization problems in Proposition 2, we make use of the PENBMI solver [68] from TOMLAB [69] integrated with the MATLAB environment through YALMIP [54].

1) $\mathcal{H}_2$- and $\mathcal{H}_\infty$-Optimal Static Decentralized Event-Based Control: This section addresses the design of optimal static

event-based controllers (i.e., without the integral action) for Σ_2. In order to regulate the walking speed of the robot, we define the discrete-time output in (15) as the robot's COM velocity evaluated on the event-based manifold[8], i.e., $z(x) := v_{\text{cm}}(x) \in \mathbb{R}^3$. In particular, we study the linearized discrete-time dynamics (16) with the quadruple of matrices $(A_{11}, E, C, 0)$ and the transfer matrix $T_{dc}(z) = C(zI - A_{11})^{-1}E$. Without employing the event-based controller, the dominant eigenvalues and spectral radius of the 17×17 Jacobian matrix of the Poincaré map (i.e., A) are $\{0.7801, -0.1788 \pm 0.6168i, -0.1215, 0.1149\}$ and 0.7801, respectively. The $\mathcal{H}_2$ and $\mathcal{H}_\infty$ norms of the transfer matrix $T_{dc}(z)$ are also 16.1137 and 23.6082. To minimize the effect of the impact model uncertainty $d[k] \in \mathbb{R}^{18}$ on the robot's center of mass velocity, we employ Part 1 of Proposition 2 with the weighting factors $w_0 = 0.01$ and $w_1 = w_2 = 2$ [we remark that $\tilde{K}_2 = 0$ as there is no integral action]. The PENBMI solver successfully converges to a set of $\mathcal{H}_2$-optimal decentralized event-based gains (i.e., K_2 and $\hat{K}_2$) for which the dominant eigenvalues and spectral radius of A_{11} become $\{0.7053, -0.0160 \pm 0.3254i, -0.2693\}$ and 0.7053, respectively (i.e., 10% improvement in the spectral radius). In addition, the $\mathcal{H}_2$ norm reduces to 10.0473 (38% improvement). We then employ Part 2 of Proposition 2 to design an $\mathcal{H}_\infty$-optimal decentralized event-based controller for the subsystem Σ_2 with the weighting factors $w_0 = 0.01$ and $w_1 = w_2 = 2$. The PENBMI solver successfully converges to a set of local gains for which the dominant eigenvalues and spectral radius of A_{11} become $\{0.7193, 0.0099 \pm 0.6112i, -0.1610\}$ and 0.7193, respectively, that corresponds to 8% improvement in the spectral radius. Moreover, the $\mathcal{H}_\infty$ norm reduces to 20.6399 (13% improvement).

2) $\mathcal{H}_2$- and $\mathcal{H}_\infty$-Optimal Dynamic Decentralized Event-Based Control: In this section, we consider dynamic decentralized event-based control design problem for Σ_2 in which the internal dynamics are taken as an integrator, see (51) and (52). We then study the linearized discrete-time dynamics (16) with the quadruple of matrices $(A_{\text{cl}}, E_{\text{cl}}, C_{\text{cl}}, 0)$ and the transfer matrix $T_{dc}(z) = C_{\text{cl}}(zI - A_{\text{cl}})^{-1}E_{\text{cl}}$. By taking $W_2 = 0_{2\times 6}$, $\hat{W}_2 = [0_{2\times 8}\, I_2]$, $w_0 = 1$ and $w_1 = w_2 = 2$ and $w_3 = 10$ for Part 1 of Proposition 2, the solver successfully converges to a dynamic $\mathcal{H}_2$ decentralized event-based controller. For this solution, the dominant eigenvalues and spectral radius of the 19×19 Jacobian matrix A_{cl} become $\{0.9540, 0.6470 \pm 0.3380i, 0.8068\}$ and 0.9540, respectively. Furthermore, the $\mathcal{H}_2$ norm reduces to 8.2992 (i.e., 49% improvement). By taking $w_0 = 2$ and $w_1 = w_2 = 2$ and $w_3 = 10$ for Part 2 of Proposition 2, the solver also converges to a dynamic $\mathcal{H}_\infty$ decentralized event-based controller for which the dominant eigenvalues and spectral radius of the Jacobian matrix A_{cl} are $\{0.9644, 0.9501, 0.5211, 0.2127 \pm 0.4339i\}$ and 0.9644, respectively. In addition, the $\mathcal{H}_\infty$ norm reduces to 13.4910 (43% improvement). Figure 2 illustrates the singular values for the 3×18 transfer matrix $T_{dc}(e^{j\omega})$ without and with employing the $\mathcal{H}_2$- and $\mathcal{H}_\infty$-optimal decentralized event-based controllers. It can be observed that by employing the above-mentioned dynamic event-based controllers, the $\mathcal{H}_\infty$ norm is decreased by 42% and (for the $\mathcal{H}_2$-optimal solution) and 43% (for the $\mathcal{H}_\infty$-optimal solution). For the above-mentioned weighting factors, we observed that the local PENBMI solver converges to dynamic decentralized feedback solutions for which the $\mathcal{H}_2/\mathcal{H}_\infty$ norms are further reduced compared to the static ones. One way to explain this norm reduction is according to [70]. In fact, [70, Theorems 1 and 3] presents *dynamic* optimal (sub-optimal) $\mathcal{H}_2/\mathcal{H}_\infty$ controllers for output feedback. Decentralized controllers in some sense are similar to output feedback as they have access to limited (i.e., local) measurements. Hence, we expect optimal dynamic decentralized controllers outperform static ones in terms of the $\mathcal{H}_2/\mathcal{H}_\infty$ norms. Figure 3 depicts the phase portraits for the yaw and roll motions of the closed-loop system with $\mathcal{H}_2/\mathcal{H}_\infty$-optimized decentralized controllers during 50 consecutive steps of walking. Convergence to the periodic orbit is clear. The animation of these simulations can be found at [71].

[8]One can choose other output functions as the absolute orientation of the robot or height of the COM evaluated on the event-based manifold.

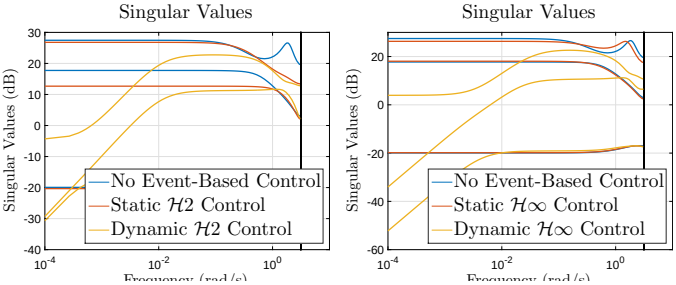

Fig. 2: Plot of the singular values for the frequency response of the 3×18 transfer matrix T_{dc} without and with employing $\mathcal{H}_2$-optimal (the left subplot) and $\mathcal{H}_\infty$-optimal (the right subplot) decentralized event-based controllers for the prosthetic leg.

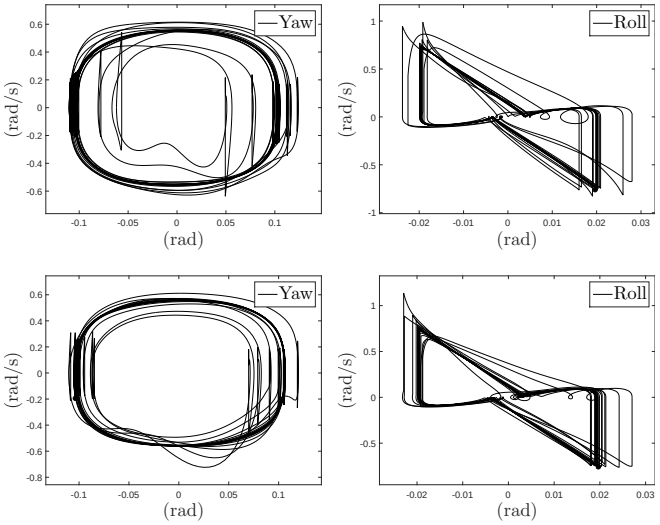

Fig. 3: Phase portraits for the yaw and roll motions of the closed-loop hybrid system with robust-optimized decentralized event-based controllers during 50 consecutive steps of walking. Top plots illustrate the phase portraits for the $\mathcal{H}_2$-optimal and dynamic update laws, whereas the bottom plots depict the phase portraits for the $\mathcal{H}_\infty$-optimal and dynamic update laws.

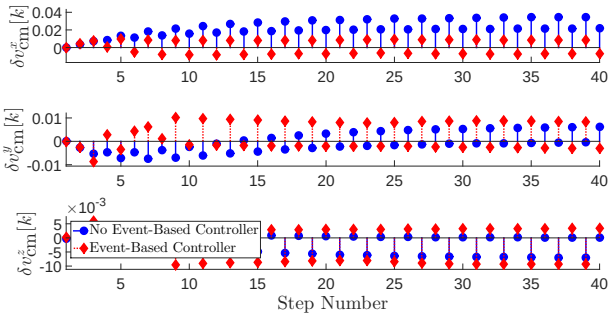

Fig. 4: Plot of the x, y, and z components of the deviation in the robot's COM velocity ($\delta c[k] = \delta v_{\text{cm}}[k]$) on the Poincaré section for a step disturbance $d[k]$ in the velocity components of the impact model. Using the $\mathcal{H}_2$-optimal dynamic decentralized event-based controller, the steady-state deviation in the lateral velocity component (i.e., x-direction) is decreased by 76% and 68% during the odd and even steps, respectively.

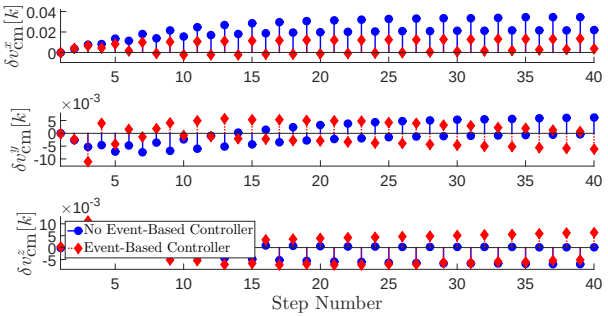

Fig. 5: Plot of the x, y, and z components of the deviation in the robot's COM velocity ($\delta c[k] = \delta v_{\text{cm}}[k]$) on the Poincaré section for a step disturbance $d[k]$ in the velocity components of the impact model. Using the $\mathcal{H}_\infty$-optimal dynamic decentralized event-based controller, the steady-state deviation in the lateral velocity component (i.e., x-direction) is decreased by 61% and 85% during the odd and even steps, respectively.

F. Robustness Against Parametric Uncertainty

In order to compare the performance of the closed-loop system with and without event-based action, we consider a step-like disturbance $d[k]$ with the magnitude of $2(\text{deg/s})$ in the velocity components of the impact map. The state solutions of the open- and closed-loop systems converge to *new stable* limit cycles, different from the original one. Figures 4 and 5 represent the x, y, and z components of the deviation in the robot's COM velocity ($\delta c[k] = \delta v_{\text{cm}}[k]$) versus the step number k. The deviation is measured with respect to the COM velocity on the Poincaré section of the original orbit. We observe a significant improvement in the lateral (i.e., side-by-side) velocity component of the robot's COM by employing the $\mathcal{H}_2$- and $\mathcal{H}_\infty$-optimal dynamic decentralized event-based controllers. In particular, for the system without event-based action, the steady-state value of δv^x_{cm} equals to 3.4631 (cm/s) and 2.1722 (cm/s) during the odd and even steps, respectively. However, the $\mathcal{H}_2$-optimal dynamic decentralized event-based controller reduces these values to 0.8602 (cm/s) for the odd steps (i.e., 75% improvement) and -0.6913 (cm/s) for the even steps (i.e., 68% improvement), see Fig. 4. In addition, the $\mathcal{H}_\infty$-optimal dynamic decentralized event-based controller reduces the deviation values to 1.3334 (cm/s) for the odd steps (i.e., 61% improvement) and 0.3614 (cm/s) for the even steps (i.e., 83% improvement), see Fig. 5. Figure 6 represents the trace of the robot's COM in the xy-plane. It is clear that the uncertainty in the impact map changes the robot's walking direction for the system without event-based action. In particular, the decentralized continuous-time controllers of [43] *cannot* reject the effect of this disturbance on the walking direction. However, the optimal dynamic decentralized event-based controllers significantly attenuate the effect of the uncertainty in the lateral velocity component and yaw motion. The animation of these simulations can be found at [71].

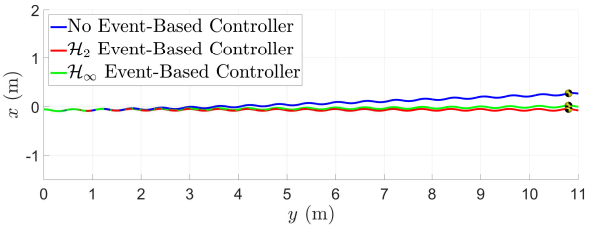

Fig. 6: Trajectory of the robot's COM in the presence of a step disturbance input $d[k]$ for the closed-loop hybrid system with and without event-based control.

G. Robustness Against Nonparametric Uncertainties

The objective of this section is to show that the proposed decentralized two-level control strategy is capable of producing stable walking gaits even if the assumptions made in the modeling of the system are not met exactly. In particular, we consider compliant contact models rather than the rigid ones assumed in the hybrid formulation of bipedal walking in (1) (i.e., nonparametric uncertainty). This leads to a continuous and compliant model to describe walking motion during the single and non-instantaneous double support phases [72]. Here, we make use of the LuGre model [73] to represent forces between the contacting surfaces. Figure 7 depicts the phase portraits of the closed-loop compliant model with the $\mathcal{H}_2$- and $\mathcal{H}_\infty$-optimal dynamic decentralized event-based controllers. The simulations start from the initial condition of Fig. 3 and the system's solution converges to *new stable* limit cycles. Unlike the phase portraits of the rigid simulator in Fig. 3, the new yaw and roll phase portraits of Fig. 7 are not symmetric with respect to the origin. We remark that the decentralized controller structure of (49)-(52) does *not* have the left-right symmetry, which yields the left-right asymmetry in the presence of parametric and nonparametric uncertainties. To compare the effect of nonparametric uncertainty on the performance of the closed-loop system with and without event-based action, Fig. 8 represents the trace of the COM in the xy-plane. We observe that the optimal dynamic decentralized event-based controllers significantly reduce the effect of nonparametric uncertainties on the robot's lateral motion and walking direction compared to the case without event-based action. The animation of these simulations can be found at

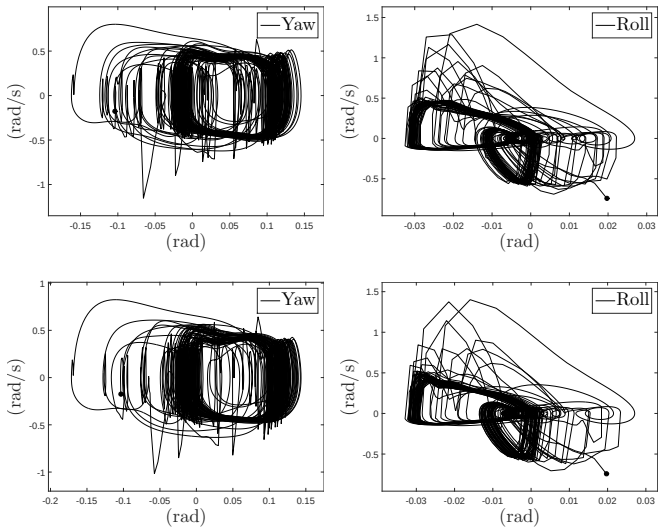

Fig. 7: Phase portraits for the yaw and roll motions of the closed-loop system during 100 consecutive steps of the compliant simulator. Top plots illustrate the phase portraits for the dynamic $\mathcal{H}_2$ update laws, whereas the bottom plots depict the phase portraits for the dynamic $\mathcal{H}_\infty$ update laws.

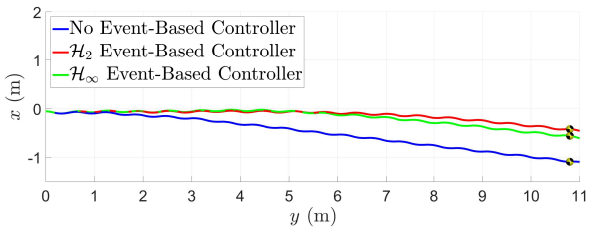

Fig. 8: Trajectory of the robot's COM for the closed-loop compliant system with and without event-based control.

[71]. One possible way to accommodate asymmetries in the yaw angle would then be to change the robot's morphology by having 3 DOFs hip joints to include yaw actuation.

VIII. Conclusion

The paper introduced a systematic framework for the design of decentralized event-based controllers to robustly stabilize periodic orbits of cooperative hybrid dynamical systems with uncertainties in discrete-time phases. A class of decentralized and two-level controllers was presented in which (1) the coordination of the subsystems is done by a common phasing variable, and (2) the parameters of continuous-time controllers are updated by static or dynamic decentralized event-based controllers. Properties of the Poincaré return map were studied for the orbital ISS. A BMI optimization framework was then developed to design $\mathcal{H}_2$- and $\mathcal{H}_\infty$-optimal decentralized event-based controllers. By design, this optimization framework can be solved with available software packages. To illustrate the power of the approach, this paper employed the theoretical results to design a decentralized two-level controller based on virtual constraints for walking of an underactuated bipedal robot with 9 DOFs and 3 degrees of underactuation. It was shown that the $\mathcal{H}_2$ and $\mathcal{H}_\infty$ norms can be reduced by 45% compared to the one-level control scheme in our previous work [43]. The paper also demonstrated that by employing the $\mathcal{H}_2$- and $\mathcal{H}_\infty$-optimal dynamic decentralized event-based controllers, the effect of impact model uncertainties on the lateral velocity and walking direction is significantly attenuated.

For future research, we will investigate other decentralized dynamic event-based controllers that go beyond simple integrators with other global sets of measurable signals to further improve the $\mathcal{H}_2$ and $\mathcal{H}_\infty$ norms. We will also investigate the scalability of the current framework to design decentralized event-based controllers for bipedal and quadrupedal walking models with higher degrees of freedom and/or underactuation. We will use this framework to design and implement controllers for powered prosthetic legs used by lower-limb amputees. A potential drawback of employing event-based stabilizing laws is that the parameter updates required for robust stability of periodic orbits are only made when the state trajectory crosses the Poincaré section. This can be partly mitigated by choosing the Poincaré section at the middle of the gait [51]. However for future work, we will investigate multiple Poincaré sections approach to design decentralized hierarchical controllers that can address a broader range of disturbances occurring at different subphases of walking gaits.

Appendix A
ISS Lyapunov Functions

Consider the nonlinear state equation $\tilde{x}[k+1] = \tilde{f}(\tilde{x}[k], \tilde{u}[k])$, $k = 0, 1, \cdots$ with the property $\tilde{f}(0,0) = 0$, where $\tilde{f} : \mathbb{R}^n \times \mathbb{R}^m \to \mathbb{R}^n$ is continuously differentiable.

Definition 4: [74] A continuous function $V : \mathbb{R}^n \to \mathbb{R}_{\geq 0}$ is said to be a local ISS-Lyapunov function for $\tilde{x}[k+1] = \tilde{f}(\tilde{x}[k], \tilde{u}[k])$ if there exist $\delta > 0$, $\mathcal{K}_\infty$ functions $\alpha_1, \alpha_2, \alpha_3$, and a $\mathcal{K}$ function σ such that (1) $\alpha_1(\|\tilde{x}\|) \leq V(\tilde{x}) \leq \alpha_2(\|\tilde{x}\|)$ for all $\tilde{x} \in \mathbb{R}^n$ with the property $\|\tilde{x}\| < \delta$ and (2) $V(\tilde{f}(\tilde{x}, \tilde{u})) - V(\tilde{x}) \leq -\alpha_3(\|\tilde{x}\|) + \sigma(\|\tilde{u}\|)$ for all $(\tilde{x}, \tilde{u}) \in \mathbb{R}^n \times \mathbb{R}^m$ with the property $\|\tilde{x}\| < \delta$ and $\|\tilde{u}\| < \delta$.

Lemma 2: Assume that $\tilde{x} = 0$ is an exponentially stable equilibrium point for the 0-input system $\tilde{x}[k+1] = \tilde{f}(\tilde{x}[k], 0)$. Then, there is a local ISS-Lyapunov function for $\tilde{x}[k+1] = \tilde{f}(\tilde{x}[k], \tilde{u}[k])$.

Proof: From the exponential stability of the origin, one can conclude that the Jacobian matrix $\tilde{A} := \frac{\partial \tilde{f}}{\partial \tilde{x}}(0,0)$ is a Schur matrix, i.e., the eigenvalues of $\tilde{A}$ are located strictly inside the unit circle. Thus, for every positive definite matrix $\tilde{Q}$, there is a unique and positive definite matrix $\tilde{P}$ which satisfies the discrete-time Lyapunov equation $\tilde{A}^\top \tilde{P} \tilde{A} - \tilde{P} = -\tilde{Q}$. In addition, $\tilde{f}$ can be written as $\tilde{f}(\tilde{x}, \tilde{u}) = \tilde{A}\,\tilde{x} + \tilde{B}\,\tilde{u} + \tilde{g}(\tilde{x}, \tilde{u})$, where $\tilde{B} := \frac{\partial \tilde{f}}{\partial \tilde{u}}(0,0)$. The function $\tilde{g} : \mathbb{R}^n \times \mathbb{R}^m \to \mathbb{R}^n$ satisfies (1) $\tilde{g}(0,0) = 0$ and (2) $\lim_{(\tilde{x},\tilde{u}) \to (0,0)} \frac{\|\tilde{g}(\tilde{x},\tilde{u})\|}{\|(\tilde{x},\tilde{u})\|} = 0$ [47, pp. 139]. In particular, for any $\varepsilon > 0$, there is $\delta > 0$ such that $\|\tilde{g}(\tilde{x}, \tilde{u})\| \leq \varepsilon (\|\tilde{x}\| + \|\tilde{u}\|)$ for all $\|(\tilde{x}, \tilde{u})\| < \delta$. Let us consider the positive definite function $V(\tilde{x}) := \tilde{x}^\top \tilde{P} \tilde{x}$ with $\alpha_1(\|\tilde{x}\|) := \lambda_{\min}(\tilde{P})\|\tilde{x}\|^2$ and $\alpha_2(\|\tilde{x}\|) := \lambda_{\max}(\tilde{P})\|\tilde{x}\|^2$. Direct computation then yields

$$V\left(\tilde{f}(\tilde{x}, \tilde{u})\right) - V(\tilde{x}) \leq -\alpha_3(\|\tilde{x}\|) + W(\|\tilde{x}\|, \|\tilde{u}\|),$$

where $\alpha_3(\|\tilde{x}\|) := \frac{1}{2}\lambda_{\min}(\tilde{Q})\|\tilde{x}\|^2$ and

$$W(\|\tilde{x}\|, \|\tilde{u}\|) := -a_{11}\|\tilde{x}\|^2 + 2a_{12}\|\tilde{x}\|\|\tilde{u}\| + a_{22}\|\tilde{u}\|^2$$

with the coefficients $a_{11} := \frac{1}{2}\lambda_{\min}(\tilde{Q}) - \varepsilon^2\|\tilde{P}\| - 2\varepsilon\|\tilde{A}^\top \tilde{P}\|$, $a_{12} := \|\tilde{A}^\top \tilde{P}\tilde{B}\| + \varepsilon^2\|\tilde{P}\| + \varepsilon\|\tilde{A}^\top \tilde{P}\| + \varepsilon\|\tilde{B}^\top \tilde{P}\| > 0$, and $a_{22} := \|\tilde{B}^\top \tilde{P}\tilde{B}\| + \varepsilon^2\|\tilde{P}\| + 2\varepsilon\|\tilde{B}^\top \tilde{P}\| > 0$. If we choose ε sufficiently small, then $a_{11} > 0$, and therefore, $W(\|\tilde{x}\|, \|\tilde{u}\|)$ becomes a quadratic and concave function with respect to $\|\tilde{x}\|$ that reaches the global maximum at $\|\tilde{x}\|_{\max} = \frac{a_{12}}{a_{11}}\|\tilde{u}\|$. To complete the proof, one can define the $\mathcal{K}$ function σ as the value of the W function at this point, i.e.,

$$\sigma\left(\|\tilde{u}\|\right) := W\left(\|\tilde{x}\|_{\max}, \|\tilde{u}\|\right) = \frac{a_{12}^2 + a_{11}\, a_{22}}{a_{11}}\|\tilde{u}\|^2.$$

■

APPENDIX B
PROOF OF THEOREM 1

From the Poincaré section's analysis [23, Theorem 4.1, pp. 89], the periodic orbit $\hat{\mathcal{O}}_a$ being exponentially stable for $\hat{\Sigma}_a^{\text{cl}}$ together with the transversality condition of Lemma 1 implies that the equilibrium point $(x, e) = (x^\star_{\text{eb}}, 0)$ is exponentially stable for (15) in the absence of the disturbance input d. Lemma 2 shows that exponential stability implies the existence of a quadratic ISS-Lyapunov function about an open neighborhood of the equilibrium point $(x, e) = (x^\star_{\text{eb}}, 0)$ of (15), and then [74, Lemma 3.5] establishes input-to-state stability for (15). In particular, there exist (i) $\delta_1 > 0$, (ii) a class $\mathcal{KL}$ function ϱ, and (iii) a class $\mathcal{K}$ function ω such that for every initial condition $x[0] \in \mathcal{N}_{\delta_1}(x^\star_{\text{eb}}) \cap \mathcal{S}^0_{\text{eb}}$ and $e[0] \in \mathcal{N}_{\delta_1}(0) \subset \mathbb{R}^l$, the state solution of (15) satisfies the following inequality

$$\left\| \begin{bmatrix} x[k] - x^\star_{\text{eb}} \\ e[k] \end{bmatrix} \right\| \leq \varrho\left(\left\| \begin{bmatrix} x[0] - x^\star_{\text{eb}} \\ e[0] \end{bmatrix} \right\|, k \right) + \omega\left(\|d\|_{l_\infty}\right) \tag{53}$$

for $k = 0, 1, \cdots$.

Now let us define the augmented and $\mathcal{C}^\infty$ vector field $\hat{f}_a^{\text{cl}}(x, e) := (f_0^{\text{cl}\top}(x, \beta^\star), 0)^\top$ for the closed-loop hybrid system (20). We remark that according to Assumption 3, the closed-loop ODE $\dot{x} = f^{\text{cl}}(x, \beta)$ in (7) is $\mathcal{C}^1$. However, the pre-update portion of the dynamics, i.e., $\dot{x} = f_0^{\text{cl}}(x, \beta^\star)$ defined for $x \in \mathcal{S}^-_{\text{eb}}$, is $\mathcal{C}^\infty$ as $\text{fcn}(x, \beta^\star)$ in (6) is $\mathcal{C}^\infty$. This satisfies [75, Assumption A.1] for the single-phase closed-loop hybrid model (20) for which the ISS property is studied (see Definition 2). In particular, the continuous-time dynamics of (20) include the pre-update phase. From Lemma 1, the reset map for the hybrid model (20) is the composition of the flow of post-update phase and the impact map which is $\mathcal{C}^1$ by construction. This satisfies [75, Assumption A.3].

The unique solution of the augmented ODE $\dot{x}_a = \hat{f}_a^{\text{cl}}(x_a)$ with the initial condition $x_a(0)$ (at time $t = 0$) is denoted by $\hat{\varphi}_a^f(t, x_a(0))$ for all $t \geq 0$ in the maximal interval of existence. From Parts (ii) and (iii) of [75, Lemma 9], there are $\delta_2 > 0$ and $c_2 > 0$ such that for all $x_a(0) = (x^\top(0), e^\top(0))^\top \in \mathcal{S}^-_{\text{eb}} \times \mathbb{R}^l$ with $\text{dist}(x_a(0), \hat{\mathcal{O}}_a) < \delta_2$, (1) the solution $\hat{\varphi}_a^f(t, x_a(0))$ transversally crosses the augmented guard $\mathcal{S}^0_{\text{eb}} \times \mathbb{R}^l$ in finite time t_0, and (2)

$$\sup_{0 \leq t < t_0} \text{dist}\left(\hat{\varphi}_a^f\left(t, x_a(0)\right), \hat{\mathcal{O}}_a\right) \leq c_2\, \text{dist}\left(x_a(0), \hat{\mathcal{O}}_a\right). \tag{54}$$

Let us define the intersection point as

$$x_a[0] := \left(x^\top[0], e^\top[0]\right)^\top := \hat{\varphi}_a^f\left(t_0, x_a(0)\right) \in \mathcal{S}^0_{\text{eb}} \times \mathbb{R}^l. \tag{55}$$

Then from (54), one can conclude that

$$\text{dist}\left(x_a[0], \hat{\mathcal{O}}_a\right) \leq c_2\, \text{dist}\left(x_a(0), \hat{\mathcal{O}}_a\right) < c_2\, \delta_2. \tag{56}$$

We remark that in our notation, $x_a(0)$ and $x_a[0]$ denote the initial condition of the state solution $\hat{\varphi}_a^f(t, x_a(0))$ and its first intersection with $\mathcal{S}^0_{\text{eb}} \times \mathbb{R}^l$, respectively. In addition, [75, Proposition 1] guarantees the existence of $0 < \xi < 1$ such that

$$\xi \left\| \begin{bmatrix} x[0] - x^\star_{\text{eb}} \\ e[0] \end{bmatrix} \right\| \leq \text{dist}\left(x_a[0], \hat{\mathcal{O}}_a\right) < c_2\, \delta_2. \tag{57}$$

From (57), we can shrink δ_2 if necessary such that $\frac{c_2\, \delta_2}{\xi} < \delta_1$. Then according to (53), (56) and (57), for any $\varepsilon > 0$, there is $0 < \delta(\varepsilon) < \delta_2$ such that for all $x_a(0) = (x^\top(0), e^\top(0))^\top \in \mathcal{S}^-_{\text{eb}} \times \mathbb{R}^l$ with $\text{dist}(x_a(0), \hat{\mathcal{O}}_a) < \delta$ and $d[k] \in \mathcal{N}_\delta(0) \subset \mathcal{D}$ with $k \geq 0$, one can conclude that $x[k] \in \mathcal{N}_\varepsilon(x^\star_{\text{eb}}) \cap \mathcal{S}^0_{\text{eb}}$ and $e[k] \in \mathcal{N}_\varepsilon(0) \subset \mathbb{R}^l$. In particular, this together with [75, Lemma 8] implies that for all $x_a(0) \in \mathcal{S}^-_{\text{eb}} \times \mathbb{R}^l$ with $\text{dist}(x_a(0), \hat{\mathcal{O}}_a) < \delta$, and $d[k] \in \mathcal{N}_\delta(0) \subset \mathcal{D}$, $k \geq 0$, there exists a state solution $\hat{\varphi}_a(t)$ of (20) defined on $[0, \infty)$ such that $\hat{\varphi}_a(0) = x_a(0)$. More precisely, we can shrink $\varepsilon > 0$ if necessary to satisfy the assumptions of [75, Lemmas 8 and 9]. Then there are the minimum and maximum values $0 < T_{\min}$ and $0 < T_{\max} < \infty$ for the time-to-update function $T^-(x)$ such that (1) $t_0 < T_{\max}$ and (2) $T_{\min} < T^{-\star} < T_{\max}$, where $T^{-\star}$ represents the nominal time-to-update function (i.e., fundamental period of $\mathcal{O}^-$). Furthermore, for all $x_a(0) \in \mathcal{S}^-_{\text{eb}} \times \mathbb{R}^l$ with $\text{dist}(x_a(0), \hat{\mathcal{O}}_a) < \delta$, and $d[k] \in \mathcal{N}_\delta(0) \subset \mathcal{D}$, $k \geq 0$[9],

$$0 < T_{\min} < t_{k+1} - t_k < T_{\max} < \infty, \tag{58}$$

where $\hat{\mathcal{T}}_a := \{0 < t_0 < t_1 < t_2 < \cdots\}$ denotes the switching times corresponding to the state solution $\hat{\varphi}_a(t)$. There is also $c_3 > 0$ such that

$$\sup_{t_k \leq t < t_{k+1}} \text{dist}\left(\hat{\varphi}_a(t), \hat{\mathcal{O}}_a\right) \leq c_3 \left\| \begin{bmatrix} x[k] - x^\star_{\text{eb}} \\ e[k] \end{bmatrix} \right\| \tag{59}$$

for $k \geq 0$, in which $x_a[k] := (x^\top[k], e^\top[k])^\top := \lim_{\tau \nearrow t_k} \hat{\varphi}_a(\tau)$.

Combining (53), (56), (57), and (59) yields

$$\begin{aligned} \text{dist}\left(\hat{\varphi}_a(t), \hat{\mathcal{O}}_a\right) \leq\ & c_3\, \varrho\left(\frac{c_2}{\xi}\, \text{dist}\left(x_a(0), \hat{\mathcal{O}}_a\right), k\right) \\ & + c_3\, \omega\left(\|d\|_{l_\infty}\right) \end{aligned} \tag{60}$$

for every $t \in [t_k, t_{k+1})$, $k \geq 0$, in which we have made use of the properties of class $\mathcal{KL}$ functions. Analogous to the proof of [75, Theorem 1], one can consider three different scenarios as (a) $t \in [t_k, t_{k+1}), k \geq 1$, (b) $t \in [t_0, t_1)$, and (c) $t \in [0, t_0)$ to relate the discrete-time k to the continuous-time t in inequality (60) which completes the proof.

APPENDIX C
PROOF OF PROPOSITION 2

Part 1: The BMI inequality (35) together with LMIs (36) and (40) results in A_{cl} being Hurwitz and $\|T_{dc}\|_{\mathcal{H}_2} < \sqrt{\mu}$ [46, Lemma 1]. Applying Schur's Lemma on LMIs (37)-(39) then yields $\|K_i\|_{\text{F}}^2 = \text{trace}(K_i^\top K_i) = \text{vec}(K_i)^\top \text{vec}(K_i) < \eta_i$,

[9] Equation (58) guarantees that there is no "Zeno" solution.

$\|\hat{K}_i\|_{\mathsf{F}}^2 = \text{trace}(\hat{K}_i^\top \hat{K}_i) = \text{vec}(\hat{K}_i)^\top \text{vec}(\hat{K}_i) < \hat{\eta}_i$, $\|\tilde{K}_i\|_{\mathsf{F}}^2 = \text{trace}(\tilde{K}_i^\top \tilde{K}_i) = \text{vec}(\tilde{K}_i)^\top \text{vec}(\tilde{K}_i) < \tilde{\eta}_i$ for $i \in \{1, 2\}$. Hence, η_i, $\hat{\eta}_i$, and $\tilde{\eta}_i$ represent dynamic upper bounds for the Frobenius norms of K_i, $\hat{K}_i$, and $\tilde{K}_i$, respectively.

Part 2: Pre and post multiplying the BMI inequality (42) by the block diagonal matrix $\left\{Q^{-1}, I, I, I\right\}$ and next applying Schur's Lemma on the result yield

$$\begin{bmatrix} A_{\text{cl}}^\top Q\, A_{\text{cl}} - Q & A_{\text{cl}}^\top Q\, E_{\text{cl}} & C_{\text{cl}}^\top \\ \star & E_{\text{cl}}^\top Q\, E_{\text{cl}} - \mu\, I & 0 \\ \star & \star & -I \end{bmatrix} < 0.$$

The discrete-time version of the Bounded Real Lemma provided in [56, Lemma 5.1] then results in A_{cl} being Hurwitz and $\|T_{dc}\|_{\mathcal{H}_\infty} < \sqrt{\mu}$.

APPENDIX D
PROOF OF THEOREM 2

From [25, Appendix D] and Assumptions 1-5, $T^-(x)$ and $T^+(x, \beta)$ are $\mathcal{C}^1$ functions at $x = \Delta(x^\star)$ and $(x, \beta) = (x_{\text{eb}}^\star, \beta^\star)$, respectively. In particular,

$$\begin{aligned} \frac{\partial T^-}{\partial x}\left(\Delta\left(x^\star\right)\right) &= -\frac{\frac{\partial \theta}{\partial x}\left(x_{\text{eb}}^\star\right)}{\frac{\partial \theta}{\partial x}\left(x_{\text{eb}}^\star\right) f_0^{\text{cl}}\left(x_{\text{eb}}^\star, \beta^\star\right)} \Phi_x^-\left(T^{-\star}\right) \\ \frac{\partial T^+}{\partial x}\left(x_{\text{eb}}^\star, \beta^\star\right) &= -\frac{\frac{\partial s}{\partial x}\left(x^\star\right)}{\frac{\partial s}{\partial x}\left(x^\star\right) f_0^{\text{cl}}\left(x^\star, \beta^\star\right)} \Phi_x^+\left(T^\star\right) \\ \frac{\partial T^+}{\partial \beta}\left(x_{\text{eb}}^\star, \beta^\star\right) &= -\frac{\frac{\partial s}{\partial x}\left(x^\star\right)}{\frac{\partial s}{\partial x}\left(x^\star\right) f_0^{\text{cl}}\left(x^\star, \beta^\star\right)} \Phi_\beta^+\left(T^\star\right) \end{aligned}$$

that result in $\frac{\partial \mathcal{F}^-}{\partial x}\left(\Delta\left(x^\star\right)\right) = \Pi^-\, \Phi_x^-\left(T^{-\star}\right)$, $\frac{\partial \mathcal{F}^+}{\partial x}\left(x_{\text{eb}}^\star, \beta^\star\right) = \Pi^+\, \Phi_x^+\left(T^\star\right)$, and $\frac{\partial \mathcal{F}^+}{\partial \beta}\left(x_{\text{eb}}^\star, \beta^\star\right) = \Pi^+\, \Phi_\beta^+\left(T^\star\right)$. These latter equations together with the chain rule complete the proof.

REFERENCES

[1] G. Song and M. Zefran, "Underactuated dynamic three-dimensional bipedal walking," in *Robotics and Automation. Proceedings IEEE International Conference on*, May 2006, pp. 854–859.

[2] J. Grizzle, G. Abba, and F. Plestan, "Asymptotically stable walking for biped robots: analysis via systems with impulse effects," *Automatic Control, IEEE Transactions on*, vol. 46, no. 1, pp. 51–64, Jan 2001.

[3] E. Westervelt, J. Grizzle, and D. Koditschek, "Hybrid zero dynamics of planar biped walkers," *Automatic Control, IEEE Transactions on*, vol. 48, no. 1, pp. 42–56, Jan 2003.

[4] I. Poulakakis and J. Grizzle, "The spring loaded inverted pendulum as the hybrid zero dynamics of an asymmetric hopper," *Automatic Control, IEEE Transactions on*, vol. 54, no. 8, pp. 1779–1793, Aug 2009.

[5] M. Spong and F. Bullo, "Controlled symmetries and passive walking," *Automatic Control, IEEE Transactions on*, vol. 50, no. 7, pp. 1025–1031, July 2005.

[6] M. Spong, J. Holm, and D. Lee, "Passivity-based control of bipedal locomotion," *Robotics Automation Magazine, IEEE*, vol. 14, no. 2, pp. 30–40, June 2007.

[7] R. Gregg and L. Righetti, "Controlled reduction with unactuated cyclic variables: Application to 3D bipedal walking with passive yaw rotation," *Automatic Control, IEEE Transactions on*, vol. 58, no. 10, pp. 2679–2685, Oct 2013.

[8] R. Gregg, A. Tilton, S. Candido, T. Bretl, and M. Spong, "Control and planning of 3-D dynamic walking with asymptotically stable gait primitives," *Robotics, IEEE Transactions on*, vol. 28, no. 6, pp. 1415–1423, Dec 2012.

[9] A. Ames, R. Gregg, and M. Spong, "A geometric approach to three-dimensional hipped bipedal robotic walking," in *Decision and Control, 46th IEEE Conference on*, Dec 2007, pp. 5123–5130.

[10] A. Ames, "Human-inspired control of bipedal walking robots," *Automatic Control, IEEE Transactions on*, vol. 59, no. 5, pp. 1115–1130, May 2014.

[11] A. Ames, K. Galloway, K. Sreenath, and J. Grizzle, "Rapidly exponentially stabilizing control Lyapunov functions and hybrid zero dynamics," *Automatic Control, IEEE Transactions on*, vol. 59, no. 4, pp. 876–891, April 2014.

[12] C. Chevallereau, J. Grizzle, and C.-L. Shih, "Asymptotically Stable Walking of a Five-Link Underactuated 3-D Bipedal Robot," *Robotics, IEEE Transactions on*, vol. 25, no. 1, pp. 37–50, Feb 2009.

[13] A. Ramezani, J. Hurst, K. Akbai Hamed, and J. Grizzle, "Performance analysis and feedback control of ATRIAS, a three-dimensional bipedal robot," *Journal of Dynamic Systems, Measurement, and Control December, ASME*, vol. 136, no. 2, December 2013.

[14] H. Dai and R. Tedrake, "Planning robust walking motion on uneven terrain via convex optimization," in *2016 IEEE-RAS 16th International Conference on Humanoid Robots (Humanoids)*, Nov 2016, pp. 579–586.

[15] I. R. Manchester, U. Mettin, F. Iida, and R. Tedrake, "Stable dynamic walking over uneven terrain," *The International Journal of Robotics Research*, vol. 30, no. 3, pp. 265–279, 2011.

[16] J. Pratt, T. Koolen, T. de Boer, J. Rebula, S. Cotton, J. Carff, M. Johnson, and P. Neuhaus, "Capturability-based analysis and control of legged locomotion, part 2: Application to M2V2, a lower-body humanoid," *The International Journal of Robotics Research*, vol. 31, no. 10, pp. 1117–1133, 2012.

[17] K. Byl and R. Tedrake, "Approximate optimal control of the compass gait on rough terrain," in *Robotics and Automation. IEEE International Conference on*, May 2008, pp. 1258–1263.

[18] C. Saglam and K. Byl, "Switching policies for metastable walking," in *Decision and Control, IEEE 52nd Annual Conference on*, Dec 2013, pp. 977–983.

[19] C. D. Remy, "Optimal exploitation of natural dynamics in legged locomotion," Ph.D. dissertation, ETH Zurich, 2011.

[20] K. Akbari Hamed and J. Grizzle, "Event-based stabilization of periodic orbits for underactuated 3-D bipedal robots with left-right symmetry," *Robotics, IEEE Transactions on*, vol. 30, no. 2, pp. 365–381, April 2014.

[21] M. H. Raibert, "Legged robots," *Communications of the ACM*, vol. 29, no. 6, p. 499514, 1986.

[22] K. Akbari Hamed and J. W. Grizzle, "Reduced-order framework for exponential stabilization of periodic orbits on parameterized hybrid zero dynamics manifolds: Application to bipedal locomotion," *Nonlinear Analysis: Hybrid Systems*, vol. 25, p. 227245, August 2017.

[23] E. Westervelt, J. Grizzle, C. Chevallereau, J. Choi, and B. Morris, *Feedback Control of Dynamic Bipedal Robot Locomotion*. Taylor & Francis/CRC, 2007.

[24] W. Haddad, V. Chellaboina, and S. Nersesov, *Impulsive and Hybrid Dynamical Systems: Stability, Dissipativity, and Control*. Princeton University Press, July 2006.

[25] T. Parker and L. Chua, *Practical Numerical Algorithms for Chaotic Systems*. Springer, 1989.

[26] J. W. Grizzle, "Remarks on event-based stabilization of periodic orbits in systems with impulse effects," in *Second International Symposium on Communication, Control and Signal Processing*, 2006.

[27] K. Sreenath, H.-W. Park, I. Poulakakis, and J. Grizzle, "Embedding active force control within the compliant hybrid zero dynamics to achieve stable, fast running on mabel," vol. 32, no. 3, pp. 324–345, 2013.

[28] M. Buehler, D. E. Koditschek, and P. J. Kindlmann, "Planning and control of robotic juggling and catching tasks," *International Journal of Robotics Research*, vol. 13, no. 12, pp. 101–118, April 1994.

[29] S. G. Carver, N. J. Cowan, and J. M. Guckenheimer, "Lateral stability of the spring-mass hopper suggests a two-step control strategy for running," *Chaos*, vol. 19, no. 2, p. 026106, 2009.

[30] J. Seipel and P. Holmes, "A simple model for clock-actuated legged locomotion," *Regular and Chaotic Dynamics*, vol. 12, no. 5, pp. 502–520, October 2007.

[31] A. Seyfarth, H. Geyer, and H. Herr, "Swing-leg retraction: a simple control model for stable running," *The Journal of Experimental Biology*, vol. 206, no. 15, pp. 2547–2555, 2003.

[32] D. Siljak, *Decentralized Control of Complex Systems*. Dover Publications, December 2011.

[33] L. Bakule, "Decentralized control: An overview," *Annual Reviews in Control*, vol. 32, no. 1, pp. 87–98, 2008.

[34] S.-H. Wang and E. Davison, "On the stabilization of decentralized control systems," *Automatic Control, IEEE Transactions on*, vol. 18, no. 5, pp. 473–478, Oct 1973.

[35] R. Goebel, R. Sanfelice, and A. Teel, *Hybrid Dynamical Systems: Modeling, Stability, and Robustness*. Princeton University Press, March 2012.

[36] Össur. POWER KNEE. http://www.ossur.com/powerknee/. [Online]. Available: http://www.ossur.com/powerknee/
[37] F. Sup, H. Varol, and M. Goldfarb, "Upslope walking with a powered knee and ankle prosthesis: Initial results with an amputee subject," *Neural Systems and Rehabilitation Engineering, IEEE Transactions on*, vol. 19, no. 1, pp. 71–78, 2011.
[38] M. Eilenberg, H. Geyer, and H. Herr, "Control of a powered ankle–foot prosthesis based on a neuromuscular model," *Neural Systems and Rehabilitation Engineering, IEEE Transactions on*, vol. 18, no. 2, pp. 164–173, 2010.
[39] R. Gregg and J. Sensinger, "Towards biomimetic virtual constraint control of a powered prosthetic leg," *Control Systems Technology, IEEE Transactions on*, vol. 22, no. 1, pp. 246–254, Jan 2014.
[40] R. Gregg, T. Lenzi, L. Hargrove, and J. Sensinger, "Virtual constraint control of a powered prosthetic leg: From simulation to experiments with transfemoral amputees," *Robotics, IEEE Transactions on*, vol. 30, no. 6, pp. 1455–1471, Dec 2014.
[41] A. E. Martin and R. D. Gregg, "Stable, robust hybrid zero dynamics control of powered lower-limb prostheses," *Automatic Control, IEEE Transactions on*, vol. PP, no. 99, pp. 1–1, 2017.
[42] A. Agrawal, O. Harib, A. Hereid, S. Finet, M. Masselin, L. Praly, A. Ames, K. Sreenath, and J. Grizzle, "First steps towards translating hzd control of bipedal robots to decentralized control of exoskeletons," *IEEE Access*, vol. 5, pp. 9919–9934, 2017.
[43] K. Akbari Hamed and R. D. Gregg, "Decentralized feedback controllers for robust stabilization of periodic orbits of hybrid systems: Application to bipedal walking," *Control Systems Technology, IEEE Transactions on*, vol. 25, no. 4, pp. 1153–1167, July 2017.
[44] ——, "Decentralized feedback controllers for exponential stabilization of hybrid periodic orbits: Application to robotic walking," in *2016 American Control Conference (ACC)*, July 2016, pp. 4793–4800.
[45] D. J. Villarreal, H. Poonawala, and R. D. Gregg, "A robust parameterization of human gait patterns across phase-shifting perturbations," *Neural Systems and Rehabilitation Engineering, IEEE Transactions on*, vol. 25, no. 3, pp. 265–278, March 2017.
[46] C. De Oliveira, J. Geromel, and J. Bernussou, "Extended $\mathcal{H}_2$ and $\mathcal{H}_\infty$ norm characterizations and controller parametrizations for discrete-time systems," *International Journal of Control*, vol. 75, no. 9, pp. 666–679, 2002.
[47] H. K. Khalil, *Nonlinear Systems*. Pearson, 3rd edition, 2001.
[48] S. Burden, S. Revzen, and S. Sastry, "Model reduction near periodic orbits of hybrid dynamical systems," *Automatic Control, IEEE Transactions on*, vol. 60, no. 10, pp. 2626–2639, Oct 2015.
[49] B. Griffin and J. Grizzle, "Nonholonomic virtual constraints and gait optimization for robust walking control," *The International Journal of Robotics Research*, vol. 36, no. 8, pp. 895–922, 2017.
[50] J. P. Reher, A. Hereid, S. Kolathaya, C. M. Hubicki, and A. D. Ames, "Algorithmic foundations of realizing multi-contact locomotion on the humanoid robot DURUS," in *Twelfth International Workshop on Algorithmic Foundations on Robotics*, 2016.
[51] J. Grizzle and C. Chevallereau, "Virtual constraints and hybrid zero dynamics for realizing underactuated bipedal locomotion," *arXiv preprint arXiv:1706.01127*, 2017.
[52] E. D. Sontag and Y. Wang, "New characterizations of input-to-state stability," *IEEE Transactions on Automatic Control*, vol. 41, no. 9, pp. 1283–1294, Sep 1996.
[53] S. Veer, M. S. Motahar, and I. Poulakakis, "Local input-to-state stability of dynamic walking under persistent external excitation using hybrid zero dynamics," in *2016 American Control Conference (ACC)*, July 2016, pp. 4801–4806.
[54] J. Lofberg, "YALMIP: a toolbox for modeling and optimization in MATLAB," in *Computer Aided Control Systems Design, 2004 IEEE International Symposium on*, Sept 2004, pp. 284–289.
[55] S. Boyd, L. E. Ghaoui, E. Feron, and V. Balakrishnan, *Linear Matrix Inequalities in System and Control Theory*. Society for Industrial and Applied Mathematics, June 1997.
[56] P. Gahinet and P. Apkarian, "A linear matrix inequality approach to $\mathcal{H}_\infty$ control," *International Journal of Robust & Nonlinear Control*, vol. 4, no. 4, pp. 421–448, 1994.
[57] P. de Leva, "Adjustments to Zatsiorsky-Seluyanov's segment inertia parameters," *J Biomech*, vol. 29, no. 9, pp. 123–1230, 1996.
[58] Y. Hurmuzlu and D. B. Marghitu, "Rigid body collisions of planar kinematic chains with multiple contact points," vol. 13, no. 1, pp. 82–92, 1994.
[59] S. Yang and Q. Li, "Inertial sensor-based methods in walking speed estimation: A systematic review," *Sensors*, vol. 37, no. 6, pp. 6102–6116, 2012.
[60] J. Lack, M. Powell, and A. Ames, "Planar multi-contact bipedal walking using hybrid zero dynamics," in *Robotics and Automation, IEEE International Conference on*, May 2014, pp. 2582–2588.
[61] K. Akbari Hamed, B. Buss, and J. Grizzle, "Exponentially stabilizing continuous-time controllers for periodic orbits of hybrid systems: Application to bipedal locomotion with ground height variations," *The International Journal of Robotics Research*, vol. 35, no. 8, August 2015.
[62] C. Chevallereau, G. Abba, Y. Aoustin, F. Plestan, E. Westervelt, C. Canudas-de Wit, and J. Grizzle, "RABBIT: a testbed for advanced control theory," *Control Systems Magazine, IEEE*, vol. 23, no. 5, pp. 57–79, Oct 2003.
[63] M. Maggiore and L. Consolini, "Virtual holonomic constraints for Euler Lagrange systems," *Automatic Control, IEEE Transactions on*, vol. 58, no. 4, pp. 1001–1008, April 2013.
[64] A. Shiriaev, A. Sandberg, and C. Canudas de Wit, "Motion planning and feedback stabilization of periodic orbits for an acrobot," in *Decision and Control. 43rd IEEE Conference on*, vol. 1, Dec 2004, pp. 290–295 Vol.1.
[65] A. Isidori, *Nonlinear Control Systems*. Springer; 3rd edition, 1995.
[66] A. E. Martin, D. C. Post, and J. P. Schmiedeler, "The effects of foot geometric properties on the gait of planar bipeds walking under HZD-based control," vol. 33, no. 12, pp. 1530–1543, 2014.
[67] A. Hereid, E. A. Cousineau, C. M. Hubicki, and A. D. Ames, "3D dynamic walking with underactuated humanoid robots: A direct collocation framework for optimizing hybrid zero dynamics," in *2016 IEEE International Conference on Robotics and Automation (ICRA)*, May 2016, pp. 1447–1454.
[68] D. Henrion, J. Lofberg, M. Kocvara, and M. Stingl, "Solving polynomial static output feedback problems with PENBMI," in *Decision and Control, and European Control Conference. 44th IEEE Conference on*, Dec 2005, pp. 7581–7586.
[69] TOMLAB optimization, http://tomopt.com/tomlab/.
[70] J. C. Doyle, K. Glover, P. P. Khargonekar, and B. A. Francis, "State-space solutions to standard $\mathcal{H}_2$ and $\mathcal{H}_\infty$ control problems," *IEEE Transactions on Automatic Control*, vol. 34, no. 8, pp. 831–847, Aug 1989.
[71] https://youtu.be/ntWTp4YwP3M.
[72] F. Plestan, J. Grizzle, E. Westervelt, and G. Abba, "Stable walking of a 7-DOF biped robot," *Robotics and Automation, IEEE Transactions on*, vol. 19, no. 4, pp. 653–668, Aug 2003.
[73] C. De Wit, H. Olsson, K. Astrom, and P. Lischinsky, "A new model for control of systems with friction," *Automatic Control, IEEE Transactions on*, vol. 40, no. 3, pp. 419–425, Mar 1995.
[74] Z.-P. Jiang and Y. Wang, "Input-to-state stability for discrete-time nonlinear systems," *Automatica*, vol. 37, no. 6, pp. 857–869, Jun. 2001.
[75] S. Veer, Rakesh, and I. Poulakakis, "Input-to-state stability of periodic orbits of systems with impulse effects via Poincaré analysis," *arXiv preprint arXiv:1712.03291*, 2017.

Kaveh Akbari Hamed (M'15) received the B.S. degree in electrical engineering from the University of Tabriz in 2004 and the M.S. and Ph.D. degrees in electrical engineering from Sharif University of Technology, Tehran, Iran in 2006 and 2011, respectively. He is currently an assistant professor in Mechanical Engineering at Virginia Tech. Prior to joining Virginia Tech in 2018, he was an assistant professor in Mechanical Engineering at San Diego State University. He was a postdoctoral research fellow working at the Department of Electrical Engineering and Computer Science of the University of Michigan from 2012 to 2014. His research interests include nonlinear and robust control, robotics, dynamical legged locomotion, hybrid systems, and optimization.

Robert D. Gregg IV (S'08-M'10-SM'16) received the B.S. degree (2006) in electrical engineering and computer sciences from the University of California, Berkeley and the M.S. (2007) and Ph.D. (2010) degrees in electrical and computer engineering from the University of Illinois at Urbana-Champaign. He joined the Departments of Bioengineering and Mechanical Engineering at the University of Texas at Dallas as an Assistant Professor in June 2013. Prior to joining UT Dallas, he was a Research Scientist at the Rehabilitation Institute of Chicago and a Postdoctoral Fellow at Northwestern University. His research is in the control of bipedal locomotion with applications to autonomous and wearable robots.